EXPERIMENTAL INVESTIGATION ON THE USE OF WATER SOLUBLE POLYACRYLAMIDES AS THICKENERS DURING CO_2 WAG EOR

A Thesis

by

FRANCISCO DEOMAR TOVAR

Submitted to the Office of Graduate and Professional Studies of
Texas A&M University
in partial fulfillment of the requirements for the degree of

MASTER OF SCIENCE

Chair of Committee,	Maria A. Barrufet
Co-Chair of Committee,	David S. Schechter
Committee Members,	Hisham Nars-El-Din
Head of Department,	Daniel Hill

August 2014

Major Subject: Petroleum Engineering

ABSTRACT

CO_2 flooding often results in poor sweep efficiency due to the high mobility ratio caused by its low viscosity. To mitigate this problem, alternate injection of water and CO_2 slugs (WAG) is widely applied. Recently, numerical simulation and core flood experiments in heavy oil indicate that the use of chemicals in the water slug may improve mobility control during WAG. Therefore, stability studies of common polymers used for EOR applications in CO_2 saturated environments becomes necessary. Also, the possibility to extrapolate the benefits observed in heavy oil to light and medium oil reservoirs needs to be assessed as they gather the majority of the existing CO_2 applications.

This thesis presents an evaluation of the use of polymers as water thickeners during CO_2. The work has been divided into three stages: An investigation on the stability of acrylamide based polymers exposed to CO_2 for 328 days at 122 °F. The determination of the MMP for the system crude oil – CO_2 using the slim tubing technique in a fast approach that employs a short column of 20 ft in length. And the execution of 12 core flooding experiments under miscible and immiscible conditions, in homogeneous and heterogeneous rock.

We conclude that polyacrylamide based polymers can resist the presence of CO_2. HPAM was able to retain 54% of its original viscosity after 215 days at 122 °F. PAM - ATBS increased its viscosity to 104% of its original viscosity after 328 days. A MMP of 1563 psia was calculated, which has a good correlation to previous laboratory measurements and EOS predictions for live oil. The core flooding experiments gave insights regarding the role of miscibility, frontal advance rate, heterogeneity and water viscosity on the viscous fingering of CO_2 into the oil and suggested that thickening the water during WAG could be beneficial in highly heterogeneous formations. The limitations to scale reservoir heterogeneity prevented us to reach a fully understanding of the process. An approach combining numerical simulation with experimental work is recommended.

DEDICATION

To my mother and my sister Francys;

For all their support and their patience.

For all the time I did not spend with them.

For all the hugs I owe them.

ACKNOWLEDGEMENTS

I would like to express my appreciation for the chair and the co-chair of my committee, Dr. Maria A. Barrufet and Dr. David S. Schechter, because of their support and guidance during the development of this work, and for encouraging me to always work harder and better. Similarly, to my committee member Dr. Hisham Nasr-El-Din, for his kind support and assistance.

Special thanks goes to Mr. John Maldonado, facilities coordinator at the Harold Vance Department of Petroleum Engineering, for the extra pair of hands he always put at my disposition and that I used many times. Thanks also go to my laboratory partners Johannes Alvarez and Travis Straub for their support, and to the staff members Stuart White, Betty Robins, John Winkler, and Jason Demshar for their timely assistance.

I would like to extend my gratitude to Chaparral Energy and to its Chief Executive Officer and Director Mr. Mark A. Fisher, for providing the funding, the reservoir oil, and the rock samples utilized in this investigation. In the same way, to Mr. James Stuphen, and SNF Floerger for donating the polymer samples.

Finally, thanks to my former undergraduate professor, Dr. Gonzalo Rojas, for his mentorship over so many years. Thanks to my former supervisor, Carlos Alvarez, and my former laboratory mentor, Emil Valero, because they introduced me to the fascinating world of enhanced oil recovery and shared with me their friendship, knowledge and skills, which has been the cornerstone of this work.

NOMENCLATURE

A	Cross sectional area
API	American Petroleum Institute
ASP	Alkali-surfactant-polymer
ATBS	2-acrylamido-terbutylsulfonic acid
CO_2	Carbon dioxide
cp	Centipoise, viscosity unit
CT	Computed tomography
E_D	Displacement efficiency
EOR	Enhanced oil recovery
EOS	Equation (s) of state
E_V	Volumetric sweep efficiency
GOR	Gas to oil ratio
HPAM	Hydrolyzed polyacrylamides
IFT	Interfacial tension
k	Absolute permeability
K	Consistency coefficient
$k_{o,w,g}$	Effective permeability to oil, water or gas
L	Length
M	Mobility ratio
MM	Millions
MMP	Minimum miscibility pressure
n	Flow behavior index
N_2	Nitrogen
NaCl	Sodium chloride

NBU	North Burbank Unit
O_2	Oxygen
OOIP	Original oil in place
PAM	Polyacrylamide
psi	Pound/in^2
PV	Pore volume
q	Flow rate
R^2	Coefficient of determination
RRF	Residual resistance factor
scf	Cubit feet at standard conditions
Scf/bbl	Cubic feet per barrel, both measured at standard conditions of pressure and temperature
S_{oi}	Initial oil saturation
$S_{or\ EOR}$	Residual oil saturation after an EOR process
$S_{or\ water}$	Residual oil saturation after water flooding
S_{or}	Residual oil saturation
STB/D	Barrel at standard conditions per day
$S_{w\ irr}$	Critical water saturation
S_{wi}	Initial water saturation
WAG	Water alternating gas
WOR	Water-oil ratio
γ	Shear rate
ΔP	Pressure drop
η	Apparent viscosity, cp
$\lambda_{o,w,g}$	Mobility to oil, water or gas
μ	Viscosity, cp
$\mu_{o,w,g}$	Viscosity of oil, water or gas
σ	Shear stress

σ_o	Yield stress

TABLE OF CONTENTS

Page

LIST OF FIGURES

Page

LIST OF TABLES

Page

CHAPTER I

INTRODUCTION

Carbon dioxide is the most used enhanced oil recovery (EOR) agent in the United States. Crude oil production from miscible CO_2 flooding increased by 24% from 2010 to 2012 to reach 308,564 STB/D, representing 40% of the total US production from EOR. Additionally, immiscible CO_2 injection accounted for other 43,657 STB/D in 2012. The growing interest in CO_2 is also reflected in an increase in the number of projects in the same period of time, the number of miscible projects went from 103 to 112, whereas the immiscible went from 5 to 8 (Journal 2012) .There are many reasons that make CO_2 the most popular agent for EOR. It reaches miscibility at a lower pressure than other commonly injected gases, such as methane, nitrogen or flue gas. It is supercritical at the pressures and temperatures of most oil reservoirs, with a liquid like density that reduces overriding problems compared with other gases. Additionally, it causes oil swelling and viscosity reduction.

Compared at the same pressure and temperature, the viscosity of carbon dioxide is two or three times higher than the viscosities of natural gas, methane, nitrogen and flue gas (Lake 2010).However, relative to water or crude oil viscosity these values are still low, which leads to unfavorable mobility ratio negatively affecting sweep efficiency and reducing incremental oil recovery. Low sweep efficiency is the main problem of using carbon dioxide as an injection fluid from a reservoir engineering standpoint. Reservoir heterogeneities exacerbate this problem as CO_2 flows through the higher permeability channels reaching the producer wells prematurely. Once breakthrough has occurred, the majority of the CO_2 injected will travel directly from the injector to the producer through the high permeability paths bypassing lower permeability zones with high oil saturation. Thus, incremental oil recovery can be increased if CO_2 mobility and conformance control are addressed successfully. The alternate injection of water and CO_2, known as WAG (water-alternating-gas), has been used extensively in the field to improve mobility control as higher water saturation leads to lower permeability to gas. Many research efforts have been put into more innovative solutions as direct CO_2

viscosification or thickening, foams and gel treatments. But none of them reached a technological maturity for field implementation in a large scale, and WAG remains as the best choice to improve CO_2 sweep efficiency even when it leaves from 35% to 65% of the OOIP in the porous media (Enick et al. 2012).

The addition of chemicals to the water during CO_2 WAG has been gaining attention in recent years. Experimental studies in Canadian heavy oil have found that substituting the water with a polymer solution, or an alkali-surfactant-polymer (ASP) blend during a CO_2 WAG scheme can increase recovery over conventional WAG in more than 15% of OOIP, while simultaneously improving CO_2 utilization (Zhang, Luo, and Huang 2010, Zhang, Huang, and Luo 2010). Similar results have been reported from simulation studies (Behzadi and Towler 2009).However, the majority of the reservoirs where CO_2 is being currently applied for enhanced oil recovery purposes are light to medium oil reservoirs instead of heavy or extra heavy oil reservoirs (Journal 2012).

The viscosity in heavy and extra heavy oil reservoirs is orders of magnitude higher than in medium and light oil reservoirs. Additionally, minimum miscibility pressure (MMP) is also higher in heavier oils. Therefore, heavy and extra heavy oil commonly exhibit lower recovery efficiency under CO_2 injection than light and medium oil reservoirs. This means that the Canadian heavy oil reservoirs where the addition of chemicals to the water during WAG has been evaluated may have more room for recovery efficiency improvement than light and medium oil reservoirs, making unrealistic to assume that the same degree of incremental recovery reported for the heavy oil reservoirs can be achieved using the same technique in light and medium oil reservoirs. However, reservoir rock featuring high degree of heterogeneity can severely affect sweep efficiency in light and medium oil reservoirs, and the addition of polymers to thicken the water during CO_2 WAG can results beneficial in such scenario, making its evaluation interesting.

On the other hand, the feasibility for the field implementation of this scheme, in light, medium, or heavy oil reservoirs will depend on the tolerance of the chemicals to the presence of CO_2. Hydrolyzed polyacrylamides (HPAM), the most used polymer in EOR applications, shows important degradation when exposed to

divalent cations and oxygen (Seright et al. 2010).Therefore, the performance of polymers as water thickeners in contact with CO_2 becomes also of interest, particularly for polyacrylamides. The importance of this matter increases if we consider that the use of polymers specially manufactured for higher resistance to harsh conditions can be economically prohibitive.

The work presented in this document can be divided in three parts. The first part, comprises an investigation on the stability of acrylamide based polymers exposed to CO_2 over the course of 328 days. Two polymers commonly used in EOR operations are reported in this investigation, a co-polymer of acrylamide and acrylate, and a co-polymer of acrylamide and 2-acrylamido-terbutylsulfonic acid (ATBS). To reduce thermal and chemical degradation, the water for polymer hydration was distilled and submitted to a stripping separation process using nitrogen. The polymer solutions were hydrated overnight in an oxygen-free environment. Subsequently, they were stored in sealed bottles and placed inside an oven at 122 °F. Parallel experiments were conducted in both nitrogen and carbon dioxide saturated environments for comparison. The bottles were removed from the oven over time and the apparent viscosity of the polymer solutions was measured and fitted to a power law rheological model. The ability of the polymer solutions to retain their original apparent viscosity over time at a fixed shear rate was used to quantify the stability of the polymer when exposed to carbon dioxide. Since the experiments were performed at room pressure the solubility of carbon dioxide in water is neglected.

The second part consisted in the determination of the MMP for the system crude oil - CO_2. This stage was performed in order to select the different pressures to carry out the subsequent core flooding experiments. The slim tube technique was followed using a faster approach with a 20 feet long coil instead of the commonly used 60 to 80 feet long coils. That modification enabled the faster execution of the experiments. Reservoir temperature and dead crude oil from the North Burbank Unit (NBU) in Oklahoma, US, were used during the MMP determination.

The last part comprised the execution of core flooding experiments to study the effect of adding polymers to the water during CO_2 WAG in medium to light oil reservoirs. 8 core flooding were performed in homogenous Bentheimer sandstone core plugs, and 4 more in heterogeneous actual reservoir sandstone from a vertical well in the NBU. Computer tomography was used to visualize the heterogeneities in the NBU vertical well core and cut heterogeneous plugs. The crude oil and temperature were the same as during the MMP determination. Reservoir and injection water were made in the laboratory based in the oil field composition. Experiments were conducted both below and above the MMP to compare the behavior under miscible and immiscible conditions.

A discussion of the outcome of the experimental work is presented addressing the effect of the presence of CO_2 over polyacrylamide based polymers stability, the advantages and disadvantages of the fast-slim tube technique and the effect on recovery factor of adding polymer to the water during CO_2 WAG. The impact of heterogeneities and miscibility in the incremental oil recovery is also debated and opportunities for future work are outlined.

CHAPTER II

BACKGROUND

THE NORTH BURBANK UNIT

The NBU is located near the City of Shidler in Osage County, OK. The field was discovered in May 1920 and covers around 18,000 – 24,000 acres. It is approximately 12 miles long and 5 miles wide. The producing zone is the Pennsylvanian age Burbank sandstone, a member of the Cherokee shale found at a depth of about 3000 ft. The reservoir is of fluvial origin, with individual river channels superimposed on and cut laterally into each other resulting in a massive sand body with few discontinuities. The oil wet reservoir features a west-northwest trending system of natural fractures which tend to increase to greater lengths under fluid injection. The fracturing pressure is 0.5 psi/ft, which is low when compared to the average fracturing pressure for most reservoirs, of approximately 0.75 psi/ft. The highest permeabilities exist in the northern portion of the field and are associated with high degree of vertical heterogeneity. Core data has shown a wide range of rock permeability from 1 md to over 1000 md. The upper zones feature the highest permeabilities overlaying a much tighter zone. Generally speaking, the southern part of the reservoir is tighter and more homogeneous than the northern sector (Zornes, Cornelius, and Long 1986, Jenneman, Moffitt, and Young 1996, Moffitt et al. 1993, Trantham and Moffitt 1982).

The Burbank sand thickness varies from 10 to 63 net feet and averages 42 ft. Porosity ranges from 0.15 to 0.25, and exceeds 0.18 in most of the area. The NBU original oil in place (OOIP) is estimated in 671 MM STB. The crude oil is light with an API gravity of 40° and a viscosity of 3 cp at reservoir temperature of 122 °F. Reservoir pressure was 1200 psi at discovery (Boneau and Clampitt 1977, Jenneman, Moffitt, and Young 1996, Moffitt et al. 1993).

Water flooding began in 1949 in the southern portion of the unit and was gradually extended towards the north until 1964, when it reached the northern end. Water flood oil recovery efficiency in some areas of the northern portion was half of the obtained in other areas, due to the effect of higher heterogeneity. A number of EOR efforts have been performed in the NBU. A small steam drive pilot was conducted in 1965 with disappointing results. A polymer flood pilot test was conducted from August 15th 1970 to September 29th 1971 with successful results. A surfactant/polymer pilot was started in 1975 with technical success but with unfavorable economics. (Pang, Fleming, and Boneau , Jenneman, Moffitt, and Young , Zornes, Cornelius, and Long). In 1980, a fresh water polymer flood project was implemented in a 1,440-acre area using polyacrylamide and aluminum citrate as crosslinking solution, resulting in considerable incremental oil recovery over water flooding. The oil production rate doubled and the water-oil-ratio (WOR) was reduced to less than half of its value before the polymer injection (Moffitt et al. 1993).

In June 2013, carbon dioxide injection was started in the NBU. The injection of 45 MMscf/day of anthropogenic CO_2 captured from a nitrogen fertilizer plant in Coffeyville, KS is expected to lead to an incremental recovery of approximately 100 MM STB. This work focuses in improving the performance of CO_2 flooding in the NBU.

ENHANCED OIL RECOVERY

Enhanced oil recovery is oil recovery by the injection of materials not normally present in the reservoir. This wide definition covers all modes of oil recovery and most oil recovery agents. Therefore, any oil that is produced by mechanisms other than the natural drive mechanisms normally acting in an oil reservoir, such as solution gas, water influx, gas cap drive, gravity drainage or fluid and rock expansion is considered a consequence of EOR processes. After primary mechanisms have been exhausted, only around 35% of the OOIP have been produced in the majority of medium to light oil reservoirs (Lake 2010). The next stage is usually water injection because of cost and availability. Water flooding enables the production of approximately an additional 20 % of OOIP. The remaining oil, which in most cases is close to half of the

OOIP, is trapped in the porous media by capillary forces which are directly proportional to interfacial tension (fluid-fluid and fluid-solid). Water-oil systems have high interfacial tension, ranging from 10 to 30 dynes/cm (Green 1998, Donaldson, Thomas, and Lorenz 1969). As a consequence of this, and considering the idealistic situation in which water is able to contact all the oil in the reservoir, it will only be able to displace a fraction of it. That fraction is known as displacement efficiency (E_D). Displacement efficiency controls the residual oil saturation behind a water front in a water flooding process.

$$E_D = \frac{\text{Amount of oil displaced}}{\text{Amount of oil contacted by displacing agent}} \quad (1)$$

However, the reality is that water is not able to contact all the oil in the reservoir and therefore the actual recovery is lower than that predicted by displacement efficiency and the residual oil saturation in relative permeability curves. The fraction of the original oil in place that the water is able to contact is known as volumetric sweep efficiency (E_V).

$$E_V = \frac{\text{Volume of oil contacted by displacement agent}}{\text{Volume of oil originally in place}} \quad (2)$$

The volumetric sweep efficiency is mainly controlled by the mobility ratio (M) between the water and the oil, and the heterogeneity of the reservoir (Eq. 3). The mobility of a phase (λ), water, oil or gas, is the quotient between the effective permeability of the rock to that fluid (k), which enables flow, and the viscosity of the fluid (μ), which opposes to flow (Eq. 4). Since water viscosity is usually below oil viscosity, water mobility tends to be higher than oil mobility inside the porous media, causing the water to bypass some of the oil, leading to a reduction of volumetric sweep efficiency. This effect is highly exacerbated by the presence of heterogeneities since the water preferentially flows through the high permeability channels leaving the lower permeability zones unswept.

$$M=\frac{\lambda_w}{\lambda_o} \tag{3}$$

$$\lambda_{o,w,g}=\frac{k_{o,w,g}}{\mu_{o,w,g}} \tag{4}$$

For water flooding, displacement efficiency is normally between 0.5 and 0.8 and volumetric sweep efficiency between 0.4 and 0.6. The recovery factor under water injection will be the product of those values, and therefore, it would range from 0.2 to 0.48, this is, from 20 to 48% of OOIP (Lake 2010).

Different exploitation schemes are implemented after water flooding in order to continue oil production and increase recovery factor. Several options are available for light and medium oil reservoirs. The selection of the EOR process that will follow the water flooding is strongly dependent on the properties of the fluids in the reservoir, the conditions of pressure and temperature, the properties and geometry of the geological trap itself, and of course, profitability. However, the availability of the fluid to be injected, environmental considerations, regulatory framework and required infrastructure, mostly for offshore projects, can also narrow the choices. In the United States, underground accumulations of carbon dioxide have made available its use for EOR operations, but it has been its superior performance as an EOR agent which has made it the top choice over the rest of the EOR processes.

Carbon Dioxide Flooding

In the US, 46 % of EOR oil production comes from the injection of carbon dioxide (Figure 1). Miscible injection dominates with 40 % and immiscible injection accounts for other 6 %. Moreover, if we exclude steam injection, in situ combustion and hot water injection, as those thermal processes target heavy oil reservoirs, CO_2 flooding is responsible for the production of 80% of the EOR oil production from the remaining medium and light oil reservoirs (Journal 2012).

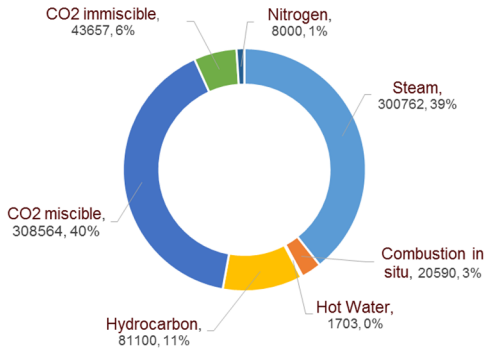

Figure 1. Crude oil production from EOR processes in the US. Production in STB/D

Miscibility plays an important role in recovery during crude oil displacement with CO_2 or any other solvent. Two components are mutually miscible if they mix in all proportions without an interface forming between them (Lake 2010). Miscibility can occur at first contact between the crude oil and CO_2, or after multiple contacts, depending on oil composition, reservoir temperature and pressure. When the conditions allow for first contact miscibility, no interface ever develops between the CO_2 and the crude oil, but instead, the displacement front will consist in a single phase that changes in composition from pure CO_2 to pure crude oil through a transition zone or mixing zone. In the case of multiple contact miscibility, an interface first exists between the CO_2 and the oil. However, vaporization of some of the lighter components of the crude oil into the CO_2 and dissolution of CO_2 into the crude oil leads to the evolution of a mixing zone that eventually replaces the interface as miscibility is developed. Most crude oil reservoirs develop miscibility after multiple contacts.

The examination of phase behavior ternary diagrams for $CO_2/C_2 - C_6/C_{7+}$ and $C_1/C_2 - C_6/C_{7+}$ systems, reveals that even when they have similar appearance, at the same pressure and temperature, the two-phase envelope is much smaller for the system containing carbon dioxide than for the one containing methane. Also, the limiting tie line for the CO_2 system tends to have a slope that is more parallel to the CO_2/C_{7+} side of the ternary diagram than the C_1 system. Thus, miscibility can be generated between CO_2 and reservoir

oils at lower pressures than between methane and reservoir oils (Green 1998). Similarly, nitrogen and reservoir oil will reach miscibility at a higher pressure than methane and reservoir oil. This condition represents the main advantage of carbon dioxide over nitrogen and methane for EOR purposes.

Under miscible conditions, given than a thermodynamic equilibrium exists at the interface and that there is no water present, the recovery efficiency approaches 100%. The presence of mobile water will reduce this efficiency by shielding or blocking the solvent from contacting some of the oil on a microscopic level leading to trapped oil saturation. When the conditions of pressure and temperature for a miscible displacement are not achieved, an interface will exist throughout the displacement process and capillary forces will retain more oil in the porous media reducing the recovery efficiency below 80 % in most cases. Under immiscible conditions, the principal mechanisms of recovery are limited amount of vaporization and extraction, oil viscosity reduction, oil swelling, solution gas drive during pressure decline and interfacial tension lowering (Lake 2010). As the degree of vaporization and extraction is a strong function of pressure and temperature, at immiscible conditions recovery will be highly dependent on reservoir pressure.

Given the impact of miscibility on recovery, knowing the conditions of temperature and pressure at which a particular crude oil/CO_2 system will achieve miscibility is a requirement in order to make any performance prediction that supports a carbon dioxide injection process. Since the temperature at reservoir conditions is usually a constant, the problem is reduced to the estimation of the minimum pressure at which the crude oil/CO_2 system would achieve miscibility. That pressure is known as minimum miscibility pressure (MMP). There are three common ways to predict MMP: empirical correlations, phase behavior calculations based on equations of state (EOS),.and laboratory experiments (Green 1998).

The use of empirical correlations is by far the easiest and fastest way to estimate MMP, but also the least accurate. Holm and Josendal (1982), Yellig and Metcalfe (1980), Glass (1985) and Yuan et al. (2005) have presented correlations to estimate MMP. Generally speaking, the correlations are based on a few reservoir parameters as temperature, molar percent of the pseudo component grouping hydrocarbons from ethane to

hexane, and the fraction of heavier components (pentanes and heavier or heptane and heavier). The temperature and oil composition of the reservoir of interest need to be inside the range of temperature and composition of the experimental data used to develop the correlation in order to obtain accurate results. However, given the complexity of hydrocarbon mixtures and the few parameters used in the correlations, there can still exist important differences in crude oil properties not taken into account that can lead to significant error.

The determination of MMP using EOS is significantly more accurate that the use of correlations, but requires the availability of crude oil composition and properties derived from laboratory tests in order to build a reliable fluid model. The more laboratory data available, the more accurate is the fluid model as it can be adjusted to match the known properties of the oil.

The slim tube technique is by far the most popular method for the experimental determination of MMP. The experiment consists in performing several displacements of crude oil by CO_2 at different pressures and at fixed reservoir temperature. The porous media consists of beads or unconsolidated sand packed in a tube of very small cross section (5/16 in) and large length (usually more than 40 ft). Every displacement is run with a fixed pressure at the outlet of the system and since the permeability of the media is high the pressure gradient is negligible. The large aspect ratio of the slim tube (length to diameter ratio) is intended to eliminate viscous fingering effects since the displacement is slow enough for all perturbations to be suppressed by transverse dispersion. Since solvent miscibility (vaporization/solubility) increases with pressure, increasing pressure leads to higher oil recovery from the slim tube, however, there is a pressure above which further pressure increase causes only a minimal increase in recovery. That pressure is regarded as the MMP from the slim tube technique. Therefore, the MMP from slim tube experiments is generally lower than the pressure required for first contact miscibility as the experimental conditions allow for the development of miscibility by multiple contacts (Lake 2010, Green 1998). Lately, the rising bubble apparatus has gained notoriety as it is able to achieve results that are close to the ones obtained using slim tube in a lower time.

Water Alternating Gas Process

Even when the viscosity of carbon dioxide is higher than the viscosity of nitrogen, methane and flue gas at reservoir conditions, it is still low when compared to the viscosity of most oils. This results in a high mobility ratio that, as discussed before for water flooding, originates a viscous fingering phenomenon that leads to low volumetric efficiency (Eq. 2-4) and reduces recovery factor. Since CO_2 viscosity is lower than water viscosity, volumetric efficiency will be generally lower for CO_2. The presence of heterogeneities in the reservoir rock greatly exacerbates this problem. Caudle and Dyes (1958) introduced the water-alternating-gas processes (WAG) as a mean to control mobility in gas floods. The technique consists in alternating the injection of specific volumes of CO_2 and water, or inject them simultaneously, in order to reduce the effective permeability of the rock to CO_2 flow as a consequence of higher water saturation. One disadvantage of this process is that the presence of mobile water shields some oil drops from being contacted by the CO_2 thus reducing the displacement efficiency. This phenomena is known as water blocking and has been reported to have a deeper effect in strongly water wet rocks (Stalkup 1970). Also, the oil production is delayed when compared to the continuous CO_2 injection. This problem has been addressed by injecting CO_2 continuously until it breaks through at the producer wells, and after that, the WAG process is implemented. This hybrid process has been successfully applied in west Texas (Green 1998). The WAG injection scheme has been extensively used on the field to improve mobility control reducing the requirements for reinjection of separated and newly purchased CO_2, as it diminish its recirculation though direct connected paths between injector and producer wells. Even when it leaves behind from 35 to 65% of OOIP, WAG remains as the state of the art for CO_2 mobility control as other techniques such as direct CO_2 thickening, foams and gels for conformance control that have been subject of considerable research efforts have had from any to limited field success (Enick et al. 2012).

Polymer Flooding and Polymer Stability

Water soluble polymers can be added to the water to improve mobility control during the water flooding process. The addition of polymers increase water viscosity reducing its mobility through the reservoir rock, increasing volumetric sweep efficiency (Eq. 2-4) and ultimate recovery factor (Green 1998, Lake 2010, Littmann 1988, Sorbie 1991). The most used polymers for EOR applications are undoubtedly polyacrylamide based polymers, which are synthetic polymers. There are also available biopolymers such as xanthan gum, and natural polymers and their derivatives such as guar gum, sodium carboxymethyl cellulose, and hydroxyl ethyl cellulose. For a polymer to be a good candidate to be used in EOR applications it should not contain oxygen in the carbon chain, for thermal stability, should have a negative ionic hydrophilic group to reduce adsorption on rock surfaces, a nonionic hydrophilic group for chemical stability, and of course, should have good viscosifying ability (Sheng 2011).

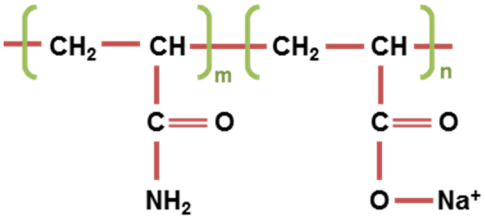

Figure 2. Molecular structure of co-polymer of acrylamide and acrylate

Polyacrylamides are manufactured by the polymerization of the acrylamide monomer, resulting in a molecule that resembles a flexible coil. To reduce the strong adsorption of polyacrylamides on mineral surfaces the polymer is partially hydrolyzed by reacting it with a base such as sodium or potassium hydroxide or sodium carbonate. Hydrolysis converts some of the amide groups ($CONH_2$) to carboxyl groups (COO-) (Sheng 2011, Green 1998). The degree of hydrolysis is the mole fraction of amide groups that are converted during the hydrolysis process and typically goes from 0.15 to 0.40 for commercial HPAM (Levitt

and Pope 2008). Therefore, the HPAM, or partially hydrolyzed polyacrylamide is a co-polymer of acrylamide and acrylate (Figure 2).

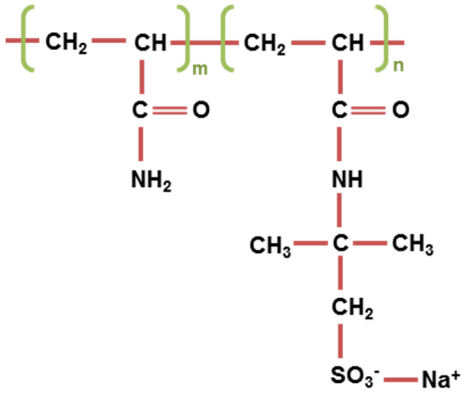

Figure 3. Molecular structure of co-polymer of acrylamide and ATBS

Oxygen and divalent cations are known to cause degradation of HPAM (Levitt and Pope 2008, Seright et al. 2010, Sheng 2011, Sorbie 1991). Oxygen combines with metals, especially ferrous iron, and residual initiators remaining from the polymerization process or other chemicals to generate free radicals. Free radicals attack and break the acrylic backbone resulting in severe viscosity reduction. This type of degradation is usually referred to as thermal degradation (Muller 1981a, b).When the reservoir temperature is above 140 °F, the hydrolysis of the acrylamide groups continues to form acrylate groups increasing the degree of hydrolysis of the polymer. If the degree of hydrolysis becomes too high, usually in excess of 0.33, and significant concentrations of divalent cations, especially calcium (Ca^{2+}), are present, the polymers can precipitate, resulting in loss of viscosity. The critical concentration of Ca^{2+} required to cause HPAM to precipitate decreases as temperature and degree of hydrolysis decreases (Levitt and Pope 2008). This degradation process is usually referred to as chemical degradation (Muller 1981a, b). Chemical degradation has been addressed by copolymerization of the acrylamide with monomer groups that resist hydrolysis, such

as ATBS (Figure 3). These polymers are more resistant to precipitation problems but they are more expensive and less efficient viscosifiers than HPAM (Seright et al. 2010).

Both the co-polymer of acrylamides and acrylate (HPAM), and the co-polymer of acrylamides and ATBS (PAM-ATBS) exhibit pseudo plastic or shear thinning behavior over the range of shear rate of interest for this investigation. The Herschel-Buckley model (Eq. 5) is a general relationship that represents the behavior of non-Newtonian fluids, where σ is the shear stress, $\dot{\gamma}$ is the shear rate, K is the consistency coefficient, n is the flow behavior index and σ_o is the yield stress (Herschel and Bulkley 1926, Steffe 1996). This model is appropriate for many fluids. The consistency coefficient is related to the thickness of the fluid and is known as viscosity (μ) for Newtonian fluids. The flow behavior index, n, represents the shear thinning (pseudo plastic) or shear thickening (dilatant) behavior. The flow behavior index is lower than 1 for pseudo plastic fluids, 1 for Newtonian fluids, and higher than 1 for dilatant fluids. To represent the behavior of shear thinning or pseudo plastic fluids the yield stress will be neglected, and Eq. 6, known as the power law relationship results. Substituting the definition of apparent viscosity (η) in Eq. 6 will yield Eq. 7, which is used to model the behavior of apparent viscosity as a function of shear rate. Apparent viscosity (η) is the preferred term to express the no constant relationship between shear stress and shear rate for a non-Newtonian fluid. Viscosity (μ) is mostly used when referring to fluids that exhibit Newtonian behavior.

$$\sigma = \mathrm{K}(\dot{\gamma})^n + \sigma_o \tag{5}$$

$$\sigma = \mathrm{K}(\dot{\gamma})^n \tag{6}$$

$$\eta = \mathrm{K}\,\dot{\gamma}^{n-1} \tag{7}$$

CHEMICALS AS WATER ADDITIVES DURING CO_2 WAG

The addition of chemicals to the water during WAG processes using CO_2 has gained some attention in recent years as they are able to improve volumetric and displacement efficiency of water. Zhang, Huang, and Luo (2010) presented a study using core flooding experiments with Saskatchewan heavy oil of 18.3 ºAPI and 353 cp in packs of unconsolidated sand produced from the reservoir. The experiments were performed under immiscible conditions at 75 ºF and 725 psi. The addition of polymer to the water slug during immiscible WAG process with CO_2 led to higher recovery when compared to continuous polymer injection and continuous CO_2 injection. Four cycles of 0.2 PV of polymer, followed with 0.2 PV slug of CO_2 and chased by 0.8 PV of water recovered a total of 18.7% OOIP over water flooding. On the other hand, the injection of 0.8 PV of polymer chased by 2.85 PV of water recovered 12.93 % OOIP, and the injection of 0.5 PV of CO2 followed by 3.51 PV of water yielded 15.30 % OOIP over water flooding. Similar experiments adding an Alkali-Surfactant-Polymer (ASP) blend also favored the addition of chemicals to the water during CO_2 WAG.

Numerical simulation results presented by Behzadi and Towler (2009) also found beneficial the addition of chemicals to the water slug during CO_2 WAG. A sector model with 20*20*3 grids with uniform dimensions of 10 ft and 30 ft of thickness was used for the runs with a crude oil of 32 ºAPI. The injection sequence was 0.1 PV of ASP chased by water and preceded by a 0.1 PV slug of CO_2, and finally followed by continuous CO_2 injection. For the conventional WAG runs the ASP slug is substituted by water. Three heterogeneous systems were investigated: coarsening upward, fining upward and random heterogeneity. The study concluded that the combination of ASP and CO_2 flooding significantly improves incremental recovery and injectivity and reduces water cut. Additionally, recovery was not substantially affected by heterogeneity.

CHAPTER III

DESCRIPTION OF EXPERIMENTS AND METHODS*

The experimental investigation presented in this thesis has been separated in three stages. The first stage, consisted in the assessment of the stability of acrylamide based polymers in the presence of CO_2. The second stage comprised the experimental determination of the M^1MP for the dead crude oil from the NBU, and the third stage consisted in the assessment of the impact of water thickening during CO_2 – WAG EOR. In this chapter, we will describe and explain the experimental design, equipment and methodology followed in each one of those stages.

LONG TERM STABILITY OF ACRYLAMIDE BASED POLYMERS IN THE PRESENCE OF CO_2

A hermetically sealable environmental bag was used to perform the experiments. After the bag has been sealed, the items inside can be manipulated using gloves located at one of its sides. All required materials and equipment were placed within the bag before starting the procedure (Figure 4).

A vacuum pump was employed to extract the air and replace it with nitrogen injected from a pressurized cylinder. During this process, we used an environmental oxygen analyzer to monitor the concentration of oxygen inside the bag. Three consecutive cycles of vacuum extraction of the gasses from the bag and nitrogen injection were performed. During the first cycle the concentration of oxygen within the bag reached 0%. The resolution of the environmental oxygen analyzer device is 0.1% O_2 and its accuracy is +0.4/-0.8% O_2.

*Part of the procedures described in this chapter have been reprinted from "Long Term Stability of Acrylamide Based Polymers During Chemically Assisted CO_2 WAG EOR" by Tovar F.D., Barrufet M.A. and Schechter D.S. SPE paper 169053. Copyright 2014 by Society of Petroleum Engineers. Reproduced with permission of SPE. Further reproduction prohibited without permission.

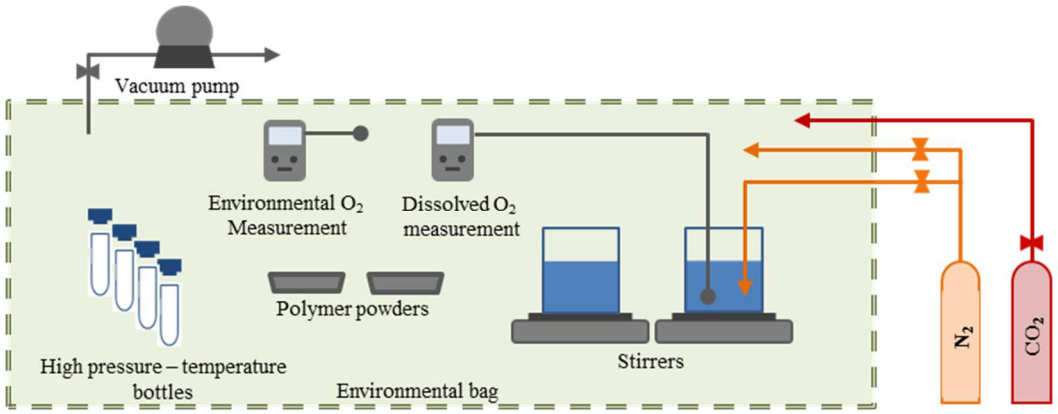

Figure 4. Schematic of the experimental set up for the assessment of polymer stability in the presence of CO_2

Two beakers containing injection water, consisting in a solution of distilled water with 500 mg/L of NaCl were placed in advance on magnetic stirrers inside the bag. The water salinity was selected to resemble the conditions of injection water used in the NBU. During the nitrogen injection phase, for each one of the cycles of gas extraction and nitrogen injection, we removed the oxygen dissolved in the injection water by means of a gas stripping process. The gas stripping process was carried out by placing a gas diffusor at the bottom of each beaker and flowing nitrogen though the injection water. A final concentration of 0.05 mg/L of oxygen was reached for each one of the beakers. The concentration of dissolved oxygen in the injection water was monitored using a dissolved oxygen measuring device provided with a galvanic sensor of 0.01 mg/L of resolution and ±0.2 mg/L of accuracy.

Two acrylamide based polymers were used in this investigation. A co-polymer of acrylamide and acrylate (HPAM) with a degree of hydrolysis ranging from 0.25 to 0.30 and an approximate molecular weight of 20 million of Dalton. And a co-polymer of acrylamide and ATBS (PAM -ATBS) with a degree of sulfonation of 0.25 and an approximate molecular weight of 8 million Dalton. Each polymer was incorporated into one of the injection water beakers and stirred during approximately 16 hours to allow hydration. The concentration of each polymer solution was 1000 mg/L. After stirring, half of the volume of each polymer

solution was distributed into 10 pressure resistant bottles and sealed in a nitrogen saturated environment. Subsequently, the vacuum pump was used to extract the nitrogen from the bag, and carbon dioxide was injected from a pressurized cylinder to replace it. Three cycles of vacuum and CO_2 injection were performed to ensure the bag was completely saturated with carbon dioxide. After that, the remaining volume of each one of the polymer solutions was distributed into 10 pressure resistant bottles in an atmosphere saturated with CO_2, and sealed. This resulted in a total of 40 bottles. 10 bottles with HPAM in contact with nitrogen, 10 bottles of HPAM in contact with CO_2, 10 bottles of PAM-ATBS with nitrogen and 10 bottles of PAM-ATBS with CO_2. The bottles have a volume of 48 cm^3 and they were filled with equal amounts of the polymer solution and the corresponding gas.

All the bottles were labeled before they were placed inside the bag. The label included the name of the polymer and either the word nitrogen or carbon dioxide depending on the aging environment. The level of polymer solution in the bottle was recorded and checked periodically to ensure that there was no leak through the cap. The bottles were removed from the bag and placed inside an oven at a constant temperature of 122 °F. The temperature was chosen as the temperature of the NBU. The apparent viscosity of the original polymer solutions was measured to be used as a baseline. The polymers were aged inside the oven for a total of 328 days. The bottles were extracted over time and the apparent viscosity and pH were measured as a function of time. The percent ratio of the apparent viscosity at a given time with respect to the apparent viscosity of the original solutions was used to quantify polymer degradation (Eq. 8).

$$\eta^{\%} = 100.\frac{\eta_t}{\eta_{t=0}} \tag{8}$$

At any time, a total of 4 bottles, one for each polymer (HPAM and PAM-ATBS), and each aging environment (N_2 and CO_2) were removed. To avoid the difficult task of suppressing completely thermal and chemical degradation, the polymers aging in nitrogen were used as a baseline to quantify the degradation for factors other than the presence of CO_2. The apparent viscosity was measured at 122 °F and room pressure

in a cone and plate, rate controlled rotational rheometer with shear rate range from 0 to 1500 sec^{-1}, and a viscosity range from 0.15 to 3,065 cp. The pH was monitored using a glass combination electrode with a range from 0 to 14 pH units, accuracy of ± 0.2 units and a resolution of 0.01 units.

MINIMUM MISCIBILITY PRESSURE DETERMINATION

The MMP determination for the CO_2 – NBU dead crude oil system followed the slim tubing technique. Dead NBU crude oil was selected, as opposed to live oil since the subsequent core flooding experiments would also use dead oil. Additionally, the current producing gas to oil ratio (GOR) in the NBU is approximately 20 Scf/bbl. The slim tube apparatus is a CORE LAB MMP 300, which consists in a dual system that host a slim tube equipment and also a core flooding equipment. Figure 6 present a partial schematic of the equipment showing the slim tube section. A particularly short packed column of 20 ft was used as coil, instead of the longer columns of more than 40 ft regularly used for slim tube experiments. This modification was introduced to reduce the time invested in each displacement. The tubing outside diameter for the column is 0.25 in and the wall thickness is 0.063 in.

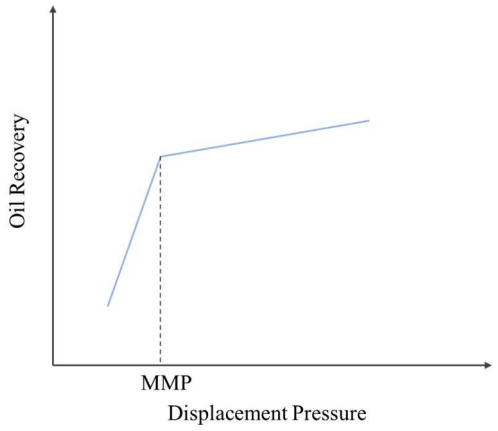

Figure 5. Schematic of oil recovery as a function of displacement pressure for MMP determination

The MMP study was conducted by displacing NBU dead crude oil with carbon dioxide. The displacement was repeated at different pressures in order to build a plot of recovery factor as a function of pressure and find the inflexion point beyond which further increase in pressure causes negligible increase in oil recovery, and therefore in displacement efficiency. The value of pressure corresponding to that inflexion point was regarded as the MMP (Figure 5).

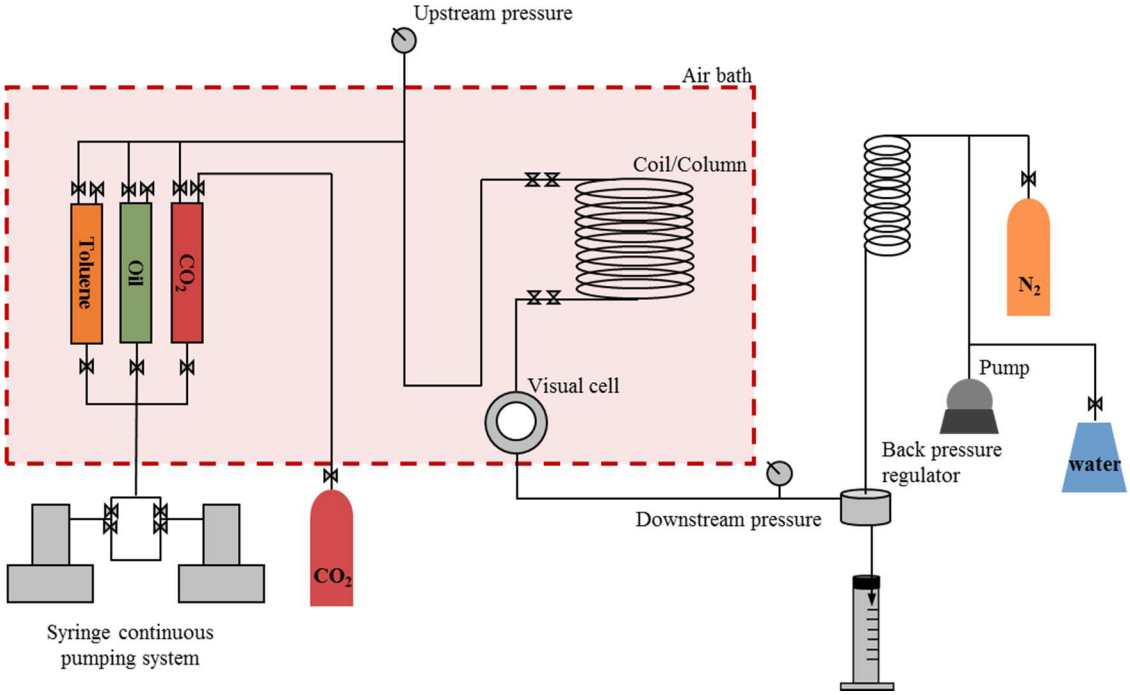

Figure 6. Schematic of the experimental set up for the MMP determination using the slim tubing technique

Before starting each displacement, we made sure the column was dry and clean by comparing its weight with its original weight. If the weight difference was less than one (1) gram, the column was connected inside the displacement equipment as shown in Figure 6. A vacuum pump was employed to remove the air inside the column and induce a negative pressure to improve subsequent oil saturation. The vacuum process

was monitored using a vacuum gauge connected in the opposite end than the vacuum pump. After at least three hours of vacuum, oil injection was started at a rate of 1 cm^3/min. During this initial oil injection stage, the air bath temperature was increased to 122 ºF. After final temperature was reached, temperature stabilization was allowed for two hours. Subsequently, back pressure was increased until the desired pressure was reached in the system.

At stabilized conditions of pressure and temperature, 2 PV of crude oil were injected through the column to completely saturate it. The injection rate was 0.2 cm^3/min. Subsequently, the oil in the column was displaced with 1.2 PV of CO_2 at a rate of 0.06 cm^3/min. The effluents were measured to calculate oil recovery factor and the data was used to build a plot as the one shown in Figure 5.

After the injection of carbon dioxide was completed, 2 PV of toluene were injected at 0.2 cm^3/min in order to remove the remaining crude oil inside the column. The toluene was removed later by injecting CO_2 at 0.2 cm^3/min during at least 12 hours. Finally, pressure and temperature are reduced to room conditions, and the column is removed from the system to measure its weight. The complete procedure was repeated 6 times at the pressures of 1000, 1500, 2000, 2500, 3000 and 3500 psi.

CORE FLOODING EXPERIMENTS

During this stage, the performance of the use of water soluble polymers as thickeners during CO_2 WAG EOR is evaluated using the core flooding technique. A series of core flooding using homogeneous Bentheimer cores and heterogeneous NBU cores were performed under miscible and immiscible conditions. For comparison purposes, core flooding experiments applying continuous CO_2 flooding, continuous polymer flooding, and conventional CO_2 WAG were also performed. The combination of all of these scenarios led to the 12 core flooding experiments presented in Table 1. The injection sequence, including volumes and concentration is discussed later.

Table 1. Core flooding experiments performed.

	Rock Type	*Miscibility Status*	*Run ID*	*Description*
Core flooding Experiments	Homogeneous rock	Immiscible displacement	1.1	Continuous CO_2 flooding
			1.2	Continuous polymer flooding
			1.3	Conventional CO_2 WAG
			1.4	Polymer assisted CO_2 WAG
		Miscible displacement	2.1	Continuous CO_2 flooding
			2.2	Continuous polymer flooding
			2.3	Conventional CO_2 WAG
			2.4	Polymer assisted CO_2 WAG
	Heterogeneous rock	Immiscible displacement	3.3	Conventional CO_2 WAG
			3.4	Polymer assisted CO_2 WAG
		Miscible displacement	4.3	Conventional CO_2 WAG
			4.4	Polymer assisted CO_2 WAG

All core flooding experiments used the same crude oil from the NBU that was used for the MMP determination. The experiments were performed at reservoir temperature of 122 ºF. Since the experimentally measured MMP was 1563 psia, the immiscible displacements were performed at 1300 psia, and the miscible ones at 1850 psia. For the conditions of pressure and temperature of all core flooding where CO_2 was injected, it was in supercritical state, so gravity override is reduced. The reservoir brine was prepared in the laboratory based on the analysis of a water sample taken from the field, the detailed composition of the reservoir brine is given later. For all experiments, injection water for water flooding consisted in distilled water with 500 mg/L of sodium chloride (NaCl). The reservoir core consisted of Bentheimer sandstone of permeability in the order of 1 Darcy for all the homogeneous runs, and NBU original reservoir cores for all the heterogeneous cores. Details on the selection of the heterogeneous cores are given later. The core diameter was 2 in for all runs and the length was 6 in for all Bentheimer sandstone core plugs, the length of the NBU reservoir core plugs was not fixed and we will elaborate more on that afterward.

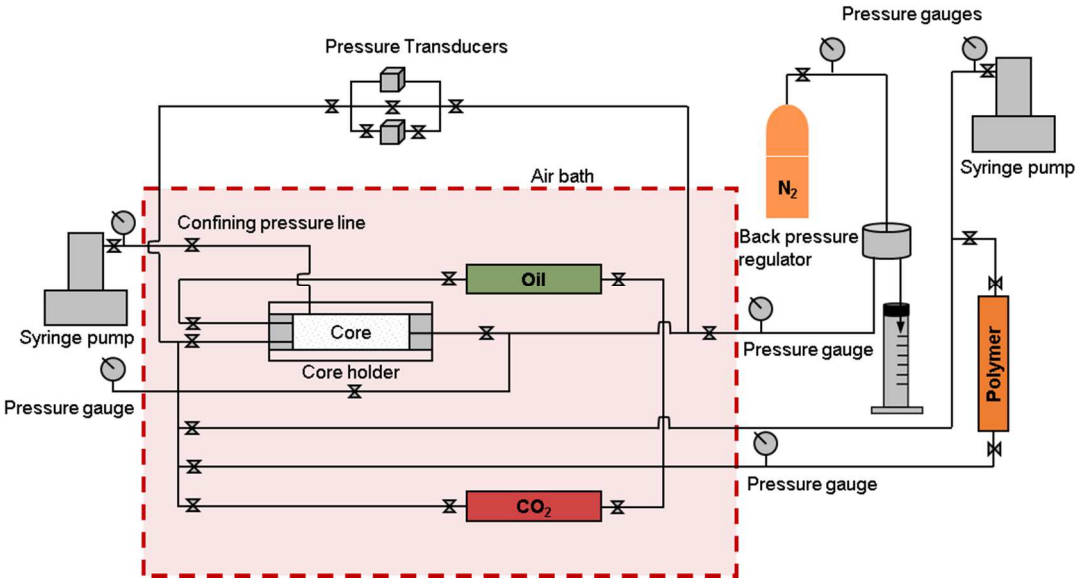

Figure 7. Schematic of the displacement equipment used for the core flooding experiments

The core flooding procedure started by packing the core plug inside a hydrostatic or biaxial core holder and applying overburden pressure of 600 psia. Porosity was then determined, and the core holder was placed horizontally inside the displacement equipment as shown in Figure 7. The system was then pressurized to reservoir pressure by increasing back pressure while injecting reservoir brine. Overburden pressure was increasing simultaneously in order to keep it 600 psi above pore pressure at all times. When reservoir pressure was reached, permeability was determined. Following that, the air bath temperature was set to 122 ^{o}F, and at least 8 hours were allowed for temperature stabilization throughout the rock and the fluids. After temperature stabilization, 1.5 PV of crude oil was pumped through the core at an advance rate of 1 ft/day to displace the reservoir brine and reach initial water saturation (S_{wi}) and original oil in place (OOIP). In all experiments, reservoir brine production ended much before than the injection of 1.5 PV of oil was completed, ensuring conditions of irreducible water saturation in the core ($S_{w\ irr}$). In selected experiments, effective permeability to oil (k_o) at S_{wi} was determined at this point.

With the core plug at initial conditions of water and oil saturation, the water flooding stage was started. 1.5 PV of water were injected at an advance rate of 1 ft/day to displace the crude oil and reach residual oil saturation conditions. In all experiments, the oil production ended much before than the duration of the water injection stage, ensuring conditions of residual oil saturation (S_{or}) before the beginning of the EOR phase. In selected runs, effective permeability to water (k_w) at conditions of residual oil saturation (S_{or}) was measured at this point.

The EOR phase was different for every run. After conditions of residual oil saturation were met, the injection of the EOR agent was started. Table 2 shows the sequence of injection during the EOR stage for each one of the experiments. For the CO_2 flooding cases (runs 1.1 and 2.1), 1 PV was selected based on common industry practices in West Texas. For the WAG processes, a tapering down scheme was chosen also following common industry practices in West Texas. With this approach, the injection of a large slug of CO_2 at the start of the flood allows for early production response, and then is followed by a slug of water for mobility control. The volume of the CO_2 slug is reduced as the project matures.

Table 2. Injection sequence during the EOR stage of the core flooding experiments

Run ID	*EOR Injection Sequence*
1.1	1 PV CO_2 + 1.5 PV chase water
1.2	1 PV polymer (600 mg/L) + 1.5 PV chase water + 3.0 PV polymer (400 mg/L) + 1.5 PV chase water + 3.0 PV polymer (800 mg/L)
1.3	0.5 PV CO_2 + 0.2 PV water + 0.3 PV CO_2 + 0.2 PV water + 0.2 PV CO_2 + 1.5 PV chase water
1.4	0.5 PV CO_2 + 0.2 PV polymer (600 mg/L) + 0.3 PV CO_2 + 0.2 PV polymer (600 mg/L) + 0.2 PV CO_2 + 1.5 PV chase
2.1	1 PV CO_2 + 1.5 PV chase water
2.2	3.5 PV polymer (600 mg/L) + 1.5 PV Chase Water
2.3	0.5 PV CO_2 + 0.2 PV water + 0.3 PV CO_2 + 0.2 PV water + 0.2 PV CO_2 + 1.5 PV chase water
2.4	0.5 PV CO_2 + 0.2 PV polymer (600 mg/L) + 0.3 PV CO_2 + 0.2 PV polymer (600 mg/L) + 0.2 PV CO_2 + 1.5 PV chase
3.3	0.5 PV CO_2 + 0.2 PV water + 0.3 PV CO_2 + 0.2 PV water + 0.2 PV CO_2 + 1.5 PV chase water
3.4	0.5 PV CO_2 + 0.2 PV polymer (600 mg/L) + 0.3 PV CO_2 + 0.2 PV polymer (600 mg/L) + 0.2 PV CO_2 + 1.5 PV chase
4.3	0.5 PV CO_2 + 0.2 PV water + 0.3 PV CO_2 + 0.2 PV water + 0.2 PV CO_2 + 1.5 PV chase water
4.4	0.5 PV CO_2 + 0.2 PV polymer (600 mg/L) + 0.3 PV CO_2 + 0.2 PV polymer (600 mg/L) + 0.2 PV CO_2 + 1.5 PV chase

For all the runs with polymer (1.2, 1.4, 2.2, 2.4, 3.4 and 4.4), a co-polymer of acrylamide-ATBS with a degree of sulfonation of 0.25 and an approximate molecular weight of 8 million Dalton was chosen based on the results of the polymer stability study. The same water used during water flooding, consisting on distilled water with 500 mg/L of NaCl was used for polymer hydration. Polymer concentration was 600 mg/L for the core flooding tests performed in homogeneous Bentheimer sandstone and 400 mg/L for the heterogeneous NBU core plugs. The guidelines followed to choose the concentration of polymer are given later in a separate section.

For the polymer flooding run below MMP (run 1.2), 1 PV of polymer was injected. Miscibility is not relevant for the polymer flooding runs (1.2 and 2.2), because CO_2 is not being injected. Pressure is also not expected to significantly impact the recovery under polymer flooding. However, polymer retention in the porous media was not measured, and it is known to reduce polymer concentration as the flood advance through the rock. The dominant mechanisms of polymer retention are adsorption on the rock and mechanical trapping in the porous media (Sheng 2011, Sorbie 1991, Littmann 1988). To compensate for polymer retention, polymer concentration was increased above the requirement to provide mobility control as explained later in a separate section addressing polymer concentration. However, after the polymer flooding run at immiscible conditions was performed (run 1.2), the low incremental oil recovery achieved raised questions about the effectiveness of the polymer concentration being used. Consequently, after the chase water stage was completed in run 1.2, an extended injection of two solutions of different polymer concentration was performed and the pressure data was recorded and employed in a second methodology to determine proper polymer concentration.

Additionally, in the polymer flooding run with reservoir pressure above MMP (run 2.2), 3 PV of polymer were injected, as opposed to the polymer flooding performed below MMP where only 1 PV was injected. Whereas this volume of polymer is unrealistic from an oil field perspective, it ensures that adsorption equilibrium is reached, discarding adsorption as a possible cause of low incremental oil recovery under polymer flooding. Polymer retention in the form of mechanical trapping was not considered to play an

important role in our experiments due to the high permeability of the Bentheimer sandstone cores and the moderate molecular weight of the polymer being used. Besides, a monotonous increment in pressure drop indicating plugging of the porous media was not detected. During all stages of production, the pressure drop was monitored and the volume of effluents were tracked in order to estimate recovery factors and saturations.

North Burbank Unit Crude Oil

Dead oil produced in the NBU field was used for the experiments. The viscosity of the oil was measured at 122 °F and room pressure in a cone and plate, rate controlled rotational rheometer with shear rate range from 0 to 1500 sec^{-1}, and a viscosity range from 0.15 to 3,065 cp. Figure 8 shows the rheogram for the dead crude oil. The linear relationship between the shear stress and the shear rate reveals the Newtonian behavior of the crude oil in the range of shear rate measured. The slope of that line corresponds to a viscosity of 3.21 cp.

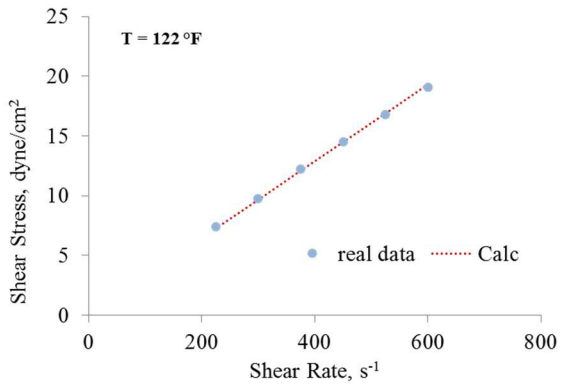

Figure 8. Rheogram for the NBU dead crude oil used in the experiments

The density and the °API of the crude oil were determined at 122 °F and room pressure in a density meter based in the oscillating U-tube method (Kratky, Leopold, and Stabinger 1974) with a measuring range from

0 to 187.28 lbm/ft^3, and a repeatability of 0.00312 lbm/ft^3. The oil has a density of 50.86 lbm/ft3, a specific gravity of 0.8377 (68 ºF) and 37.42 ºAPI (68 ºF).

Reservoir Brine

The reservoir brine was prepared in the laboratory based on the composition of the water produced in the NBU area. The analysis of a sample from a depth of 2879 ft with a gravity of 1.1362 taken in 8/17/1934 was used as reference for the original composition of the reservoir brine. Table 3 shows the concentration of the main components of the field brine and the composition of the reservoir brine used for the experiments.

Table 3. Composition of the brine from the field and the brine prepared in the laboratory and used in the experiments

		Concentration, mg/L	
Component	*Molecular Formula*	*Field Brine*	*Laboratory Brine*
Sodium	Na^+	31909	35897
Potassium	K^+	20000	22595
Calcium	Ca^{++}	13896	14591
Magnesium	Mg^{++}	2172	2281
Chlorides	Cl^-	110881	108294
Bicarbonates	CHO_3^-	32	27
Sulfates	SO_4^{--}	127	108
	Total	179017	183793

As can be noticed in Table 3, the composition of the brine used for the experiments is slightly different to the composition of the field brine. The reason for the difference is that only the concentration of the main components of the field brine is known, ignoring the contribution of the ions present in minor quantities to the ionic balance of the water. In order to avoid precipitation problems, the composition of the main components was altered to guarantee ionic balance in the laboratory brine, compensating the role of the unknown ions present in minor quantities.

Reservoir Rock

Both homogeneous and heterogeneous rocks were used during the core flooding experiments. The homogeneous cores consisted in Bentheimer sandstone with a nominal permeability of 1 Darcy. All Bentheimer core plugs had the same dimensions, 6 in length and 2 in diameter. Even though no porous media is strictly homogeneous, the Bentheimer sandstone used did not present evident heterogeneities such as changes in permeability, fractures, vugs or bedding planes that could be detected by visual examination or by the use of computed tomography scanning (CT Scanning). Moreover, the absolute permeability and porosity values measured for these core plugs were similar.

The heterogeneous rock consisted in core plugs extracted from the vertical well NBU 48-28, drilled in the North Burbank Unit. To select the depth to extract the plugs, 12 ft of whole core with 4 in diameter were imaged using CT scanning. A medical CT scanner of 16 - row detectors, with a high resolution of 0.5 mm, and double slice technology that delivers 32 slices per rotation, was used to image the NBU cores. Figure 9 shows the CT images of the cores evidencing the drastic changes in rock type, permeability and the presence of bedding planes. The plugs were cut to capture those heterogeneities in the places indicated by the white arrows.

The depth and length of the core plugs extracted from the NBU 4828 well are shown in Table 4. All core plugs had a diameter of 2 in. The runs 3.3 and 3.4 used the same core plugs, samples NBU 4828 – 1 and NBU 4828 – 2. Similarly, runs 4.3 and 4.4 used plugs NBU 4828 – 3 and NBU 4828 – 4. The core plugs were cleaned with toluene using the Dean - Stark method to be reused (Dean and Stark 1920). Due to their brittle nature, the cores NBU 4828 – 1 and NBU 4828 – 2, were fractured at their ends while they were being unpacked from the core holder, after the core flooding run number 3.3. Therefore, for run 3.4, the cores were resized and their new lengths are presented in Table 4 as NBU 4828 – 1.1 and NBU 4828 – 2.1. To reach the desired core length for the flooding experiments with actual NBU core plugs, it was necessary to build composite cores by connecting two core plugs. Filter paper was employed between the individual segments

of each composite core to improve capillary connectivity and therefore reduce the saturation disturbances caused by capillary discontinuity between the two individual core segments (Hinkley and Davis 1986, Nadeson et al. 2001).

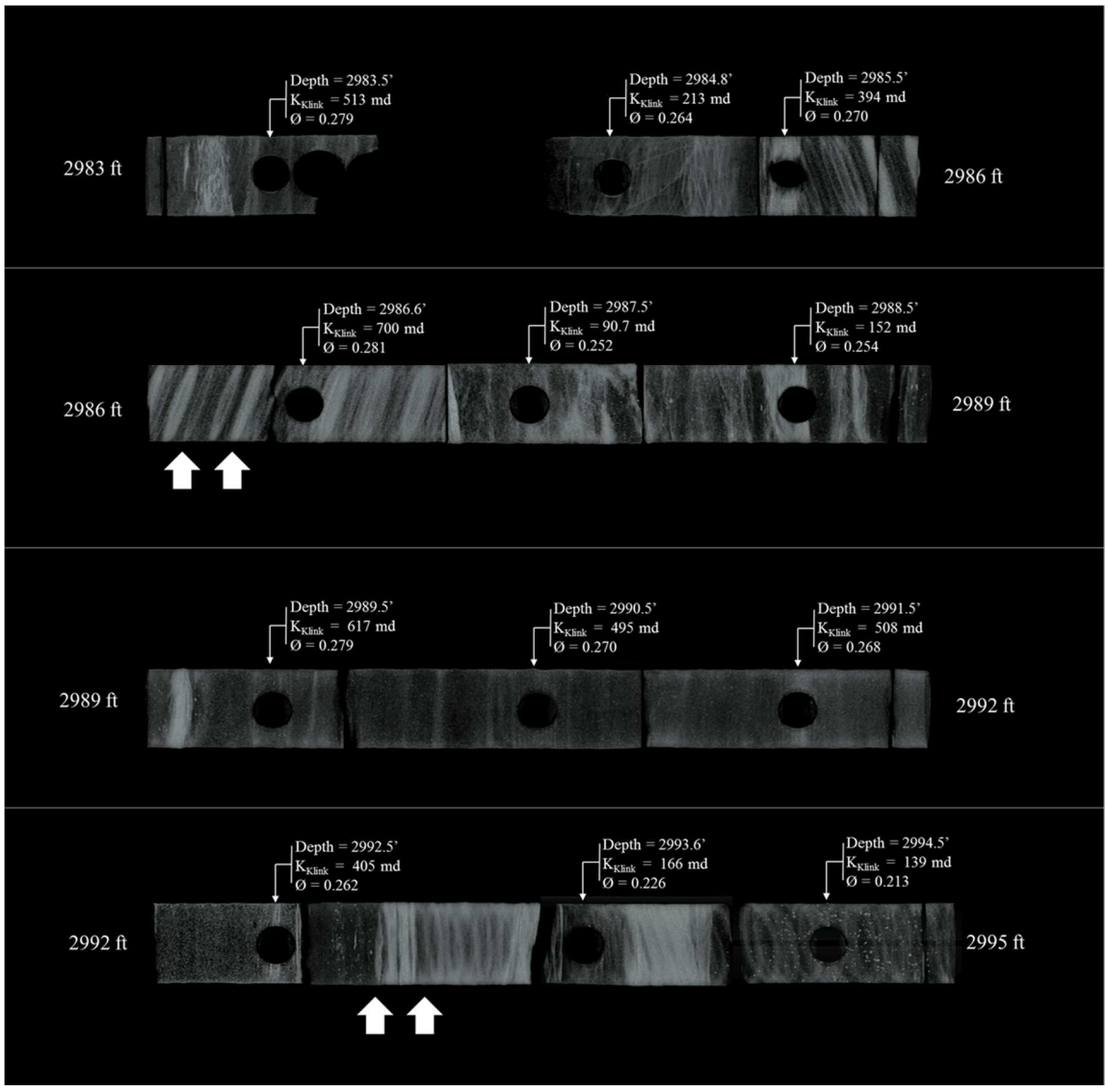

Figure 9. CT images of 14 ft of NBU core from the vertical well NBU 4828 showing the heterogeneities and the depths where the plugs were taken from.

Table 4. Depth and length of the core plugs extracted from the vertical well NBU 4828. Core diameter was 2 in for all cases.

Sample ID	*Depth, ft*	*Length, in*
NBU 4828 – 1	2986.13	2.82
NBU 4828 – 1.1	-	1.64
NBU 4828 – 2	2986.33	3.16
NBU 4828 – 2.1		2.62
NBU 4828 – 3	2992.83	3.05
NBU 4828 - 4	2993.50	3.02

To improve the flow transition between individual segments of the composite core, the bedding planes and heterogeneities were oriented in a similar fashion for the two cores comprising the same composite plug using CT. Figure 10 shows images of both composite plugs illustrating the heterogeneities and their orientation.

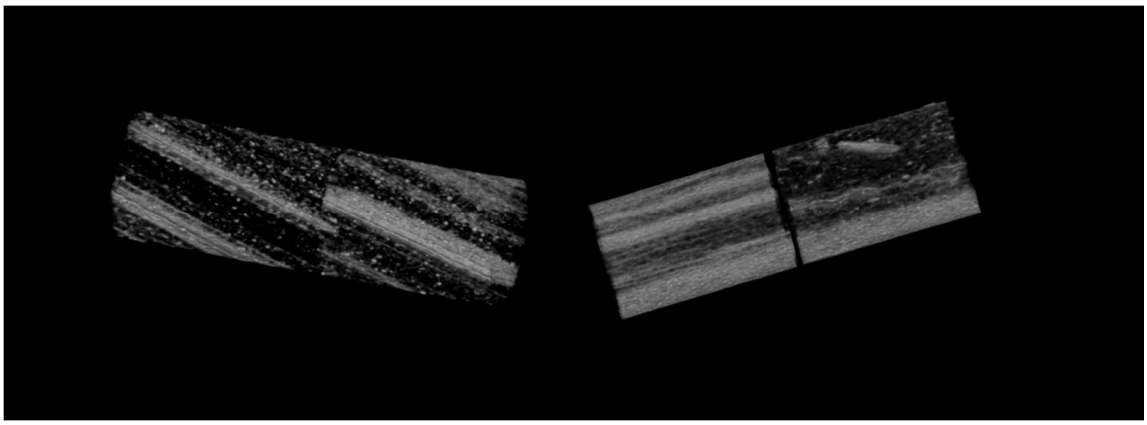

Figure 10. Composite core plugs from the well NBU 48-28 used for the heterogeneous runs. Left: cores NBU 4828 - 1 and NBU 4828 - 2. Right: cores NBU 4828 - 3 and NBU 4828 - 4.

Porosity

The porosity and pore volume were calculated in order to determine recovery factor, saturations and volume of fluids to be injected. After the core sample was packed inside the core holder and overburden pressure of 600 psi had been applied, the core holder was submitted to vacuum for a period of one hour. To confirm that the core plug was under vacuum conditions, a vacuum gauge was connected at the opposite end to the end where the vacuum pump was connected. After one hour of vacuum, reservoir brine was allowed to flow inside the core from a graduated cylinder. The change in the water volume in the graduated cylinder, after deducing the dead volume in the lines and the core holder, was equal to the pore volume of the core sample. The porosity was then obtained by dividing the pore volume by the bulk volume of the cylindrical core plugs.

Permeability

The determination of permeability was made under steady state conditions using the Darcy relationship. Equation 9 presents Darcy equation for linear flow in a porous media (Craft 1991). In this equation, the flow rate (q) is in cm^3/s, the viscosity (μ) is in cp, the pressure drop (ΔP) is in atm, the length (L) is in cm and the cross sectional area (A) is in cm^2.

$$k = \frac{q\ \mu L}{\Delta P\ A} \tag{9}$$

For the determination of absolute permeability, after the core holder was mounted inside the displacement equipment, overburden pressure had been applied and reservoir pressure had been reached, reservoir brine was flown through the core plug at different rates. For each flow rate, the stabilized pressure drop through the core was recorded. Since the dimensions of the core and the viscosity of the water are known, a plot like the one shown in Figure 11 will have the absolute permeability as the slope. The absolute permeability was

determined at room temperature to make the pressure drop value higher and therefore more accurately measurable as a consequence of the higher water viscosity.

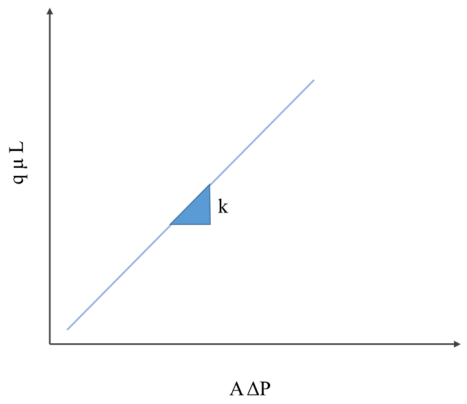

Figure 11. Schematic of plot for absolute permeability determination under steady state conditions

The effective permeability determination followed the same approach. Absolute permeability (k) and viscosity (μ) are replaced in Equation 9 and Figure 11 by effective permeability (k_o, k_w) to oil or water and viscosity (μ_o, μ_w) of oil or water. Since the determination of effective permeability was made at initial water saturation (S_{wi}) for oil permeability, and residual oil saturation (S_{or}) for water permeability, the flow rate through the porous media corresponds to the rate of the phase being injected. The effective permeability was determined at reservoir temperature.

Polymer Concentration

To estimate the polymer concentration, it was assumed that an oil bank is generated during a polymer flooding process. Therefore, ahead of the polymer front, the oil bank being displaced flows under conditions of initial water saturation, and the polymer slug behind the polymer front flows under conditions of residual oil saturation. Making this assumption, allowed the use of the effective permeabilities to oil and water

determined during the core flooding experiments in Eq. 10. Solving Eq. 10 for water viscosity provides for the viscosity required for the water in order to achieve the same mobility as the crude oil, and therefore, the displacement would be done under a mobility ratio equal to the unity.

$$M = \frac{\frac{k_{w\,(S_{or})}}{\mu_w}}{\frac{k_{o\,(S_{wi})}}{\mu_o}} = 1 \tag{10}$$

After the target viscosity for the water is estimated, it is necessary to establish a relationship between polymer concentration and water viscosity, in order to calculate the concentration of polymer required to reach the desired water viscosity. Three solutions of the selected co-polymer of acrylamide and ATBS were prepared in injection water consisting of distilled water with 500 mg/L of NaCl. The concentration of the solutions was 500, 800 and 1200 mg/L. Their viscosity was measured at room pressure and 122 ºF in a rate controlled cone and plate rotational rheometer and fitted to a power law model (Eq. 6-7) as presented in Figure 12.

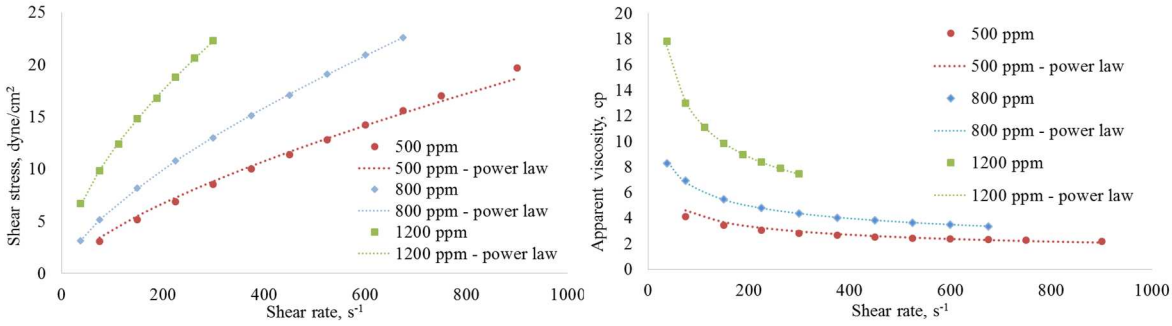

Figure 12. Rheogram (left) and viscosity curve (right) for solutions of 500, 800 and 1200 mg/L of co-polymer of acrylamide and ATBS in injection water. Measured at room pressure and 122 ºF.

$$\sigma = K(\dot{\gamma})^n \quad (11)$$

$$\eta = K\,\dot{\gamma}^{n-1} \quad (12)$$

Table 5. Power law fitting parameters for solutions of 500, 800 and 1200 mg/L of co-polymer of acrylamide and ATBS in injection water.

Concentration, mg/L	*Flow behavior index, n*	*Consistency coefficient, K, dyn.s^n/cm^2*
500	0.6795	0.1835
800	0.6770	0.2745
1200	0.5878	0.7781

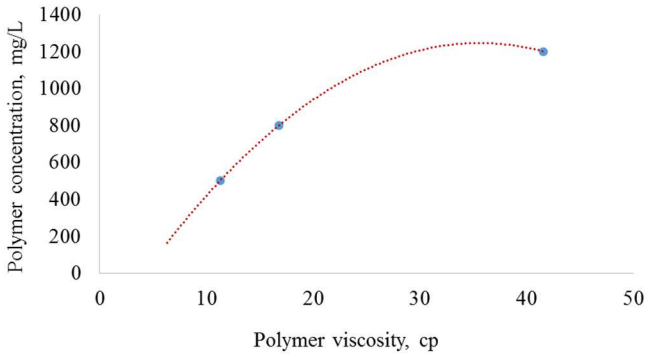

Figure 13. Polymer concentration as a function of polymer viscosity at a fixed shear rate of 4.5746 s-1 and 122 ºF. Bentheimer sandstone.

The consistency coefficient (K) and the flow behavior index (n) obtained from fitting the measured data to the power law relationship (Table 5) enabled the calculation of the viscosity of each one of the solutions at any shear rate of interest. Therefore, a plot of viscosity as a function of concentration (Figure 13) was made at a fixed shear rate of 4.5746 s^{-1}, corresponding to the shear rate imposed to the polymer solution when it flows at a velocity of 1 ft/day through the Bentheimer sandstone. The details for the estimation of the shear rate in a porous media are given thereafter. Using the data in Figure 13, a concentration of polymer of 377

mg/L is calculated to reach the target water viscosity of 9.34 cp for the displacement in the Bentheimer sandstone. Repeating the same procedure for the NBU core plugs, the same rate of advance of 1 ft/day corresponds to a shear rate of 6.9872 s^{-1}, and a required concentration of 185 mg/L of co-polymer of acrylamide and ATBS is obtained.

Since a series of assumptions has been made to reach these concentration values, and polymer adsorption and retention in the porous media have not been taken into consideration, the polymer concentration used in the experiments were 600 mg/L for the homogeneous Bentheimer sandstone and 400 mg/L for the heterogeneous NBU sandstone.

The shear rate in the porous media was estimated using the Christopher and Middleman (1965) expression for flow of a power law fluid through a packed tube (Eq.11) where the shear rate at the wall (γ_w, s^{-1}) is a function of the flow behavior index from the power law model (n), the flow rate (q, cm^3/sec), the cross sectional area (A, cm^2),the porosity (ø) and the permeability of the media (k, cm^2).

$$\dot{\gamma}_w = \frac{3n+1}{4n} \frac{12\,q}{A[150\,k\,\phi]^{1/2}} \tag{11}$$

To use the equation, the permeability and the porosity were taken from the laboratory measurements for the Bentheimer sandstone and the NBU sandstone, and converted to the proper units ($1cm^2 \approx 10^{11}$md). The non-linearity related to the flow behavior index (n) is addressed by assuming a value of 0.67 for equation 11, based on the data on Table 5. And the cross sectional area of the core is fixed and known.

A second methodology, based on experimental measurements, was also used for polymer concentration estimation in the homogeneous Bentheimer cores (Pandey et al. 2008, Manji and Stasiuk 1988). The mobility ratio (Eq. 10) can be expressed as a function of pressure, flow rate and core dimensions using the Darcy equation (Eq. 9). Therefore, the polymer solution will have the same mobility as the oil for a concentration

that provides the same ratio of pressure drop to flow rate than the oil does, given that cross-sectional area and core length are similar.

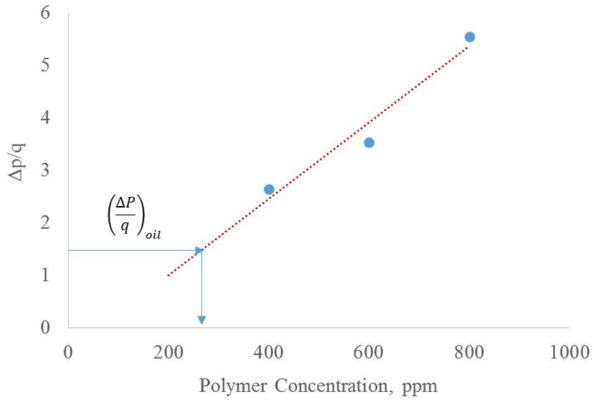

Figure 14. Ratio of pressure drop to rate as a function of polymer concentration for three polymer solutions in Bentheimer sandstone

After the polymer flooding performed at pressure below the MMP of the system crude oil/CO_2 was completed, an aqueous solution with a polymer concentration of 400 mg/L was flown followed by water, and after that, a third solution of 800 mg/L of polymer was injected. Since the actual polymer flooding was performed at a concentration of 600 mg/L, we collected pressure drop data for three different polymer concentrations. That data was used to build a plot of the ratio of pressure drop to rate as a function of polymer concentration (Figure 14). The rate is not relevant in this case since all displacements were performed at similar advance rate of 1 ft/day. Entering the plot using the ratio of pressure drop to rate for the crude oil, obtained after the drainage stage, an optimal polymer concentration close to 300 mg/L can be estimated. This polymer concentration is in agreement with the 377 mg/L estimated using the methodology previously described.

Contact Angle

The contact angle was measured for both the homogeneous Bentheimer cores and the NBU heterogeneous cores. Whereas the contact angle measurement cannot be considered as a part of the core flooding experiments, they are described at this point as they support the analysis of such experiments. The contact angle was measured with a video based optical contact angle measuring instrument. The measuring range for contact angle goes from 0 to 180º and the video system has a measuring precision of ± 0.1º. The measurements were performed at reservoir temperature of 122 ºF using the captive drop method (Figure 15). The captive drop method enable the measurement of water/oil/rock contact angle by the use of a specially shaped needle to deliver the crude oil drop underneath the surface of the rock, in the presence of an aqueous higher density phase. All the measurements used NBU crude oil and the reservoir brine prepared in the laboratory.

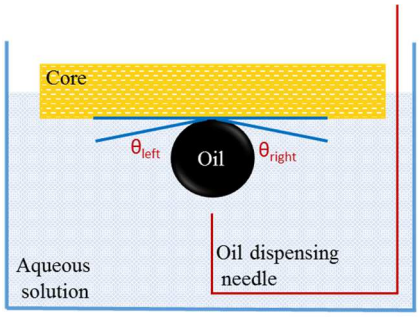

Figure 15. Schematic representation of captive drop method for contact angle determination

CHAPTER IV

PRESENTATION AND DISCUSSION OF RESULTS*

LONG TERM STABILITY OF ACRYLAMIDE BASED POLYMERS IN THE PRESENCE OF CO_2

The rheograms and the viscosity cu[2]rves of the original solutions of HPAM and PAM-ATBS are shown in Figure 16. Both polymers exhibit pseudo plastic behavior over the range of shear rate measured and, therefore, the power law equation (Eqs. 6 - 7) was used to fit the relationship between shear stress (σ) and shear rate (γ ˙).The polymer solutions have similar concentration of 1000 mg/L, however, the HPAM exhibit higher viscosity than the PAM-ATBS as a consequence of the addition of the ATBS fraction, as mentioned earlier.

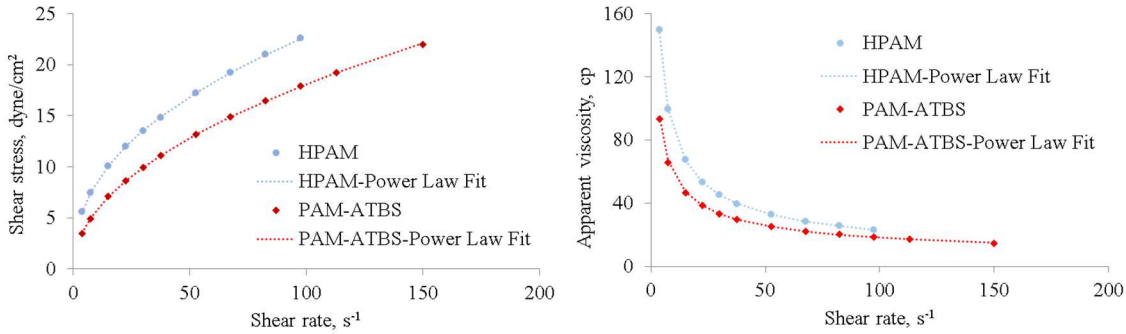

Figure 16. Rheograms (left) and viscosity curves (right) for HPAM and PAM-ATBS at zero time and 122 F. Viscoelastic behavior is observed.

*Part of the results presented in this chapter have been reprinted from "Long Term Stability of Acrylamide Based Polymers During Chemically Assisted CO_2 WAG EOR" by Tovar F.D., Barrufet M.A. and Schechter D.S. SPE paper 169053. Copyright 2014 by Society of Petroleum Engineers. Reproduced with permission of SPE. Further reproduction prohibited without permission.

The apparent viscosities presented in Figure 16 will be used as baseline to quantify the changes in apparent viscosity over time for the polymer solutions stored at reservoir temperature. The apparent viscosity change is expressed as a percentage ratio of the apparent viscosity at any given time to the original apparent viscosity of the same solution (Eq. 8), and is used in this investigation to indicate polymer stability. Since apparent viscosity is a function of shear rate for pseudo plastic fluids, a fixed shear rate of 20 sec^{-1} was selected as the flow in porous media occurs at low shear rate. A lower value was not used because the accuracy of the viscosity measurements in our rheometer diminishes at very low shear rates. For all the viscosity measurements performed, a regression was made to adjust the parameters in the power law equation (Eq. 2). The resulting consistency coefficient (K) and flow behavior index (n) are presented in Table 6 for all polymer solutions at every time step. The coefficient of determination (R^2) is also presented to indicate the quality of the data fitting.

Table 6. Power law model parameters for all solutions at every time. The consistency coefficient K is given in dyne.s^n/cm^2

Aging time, days	*HPAM*						*PAM-ATBS*					
	Nitrogen			*Carbon Dioxide*			*Nitrogen*			*Carbon Dioxide*		
	K*	*n*	R^2	K	*n*	R^2	K	*N*	R^2	K	*n*	R^2
0	3.124	0.431	1.000	3.124	0.431	1.000	1.848	0.495	1.000	1.848	0.495	1.000
1	7.107	0.267	0.995	2.302	0.440	1.000	4.284	0.342	0.998	3.308	0.387	1.000
5	4.042	0.372	0.999	1.226	0.515	0.999	4.041	0.362	0.999	1.727	0.475	1.000
18	2.434	0.461	1.000	0.877	0.484	0.993	3.282	0.404	1.000	1.012	0.550	0.999
31	3.107	0.425	1.000	2.015	0.433	0.998	3.558	0.367	0.999	1.889	0.473	0.999
80	0.816	0.658	0.999	0.735	0.624	0.999	3.257	0.404	1.000	1.470	0.533	0.999
119	1.557	0.577	0.997	2.060	0.446	0.999	3.354	0.401	0.999	1.955	0.474	0.999
159	2.135	0.486	0.999	1.373	0.517	0.999	3.497	0.387	1.000	2.208	0.450	1.000
187	3.464	0.419	0.999	0.569	0.667	1.000	3.653	0.367	1.000	1.834	0.483	1.000
215	2.269	0.483	0.999	1.635	0.483	0.999	3.559	0.374	1.000	1.638	0.488	1.000
328	0.068	0.891	1.000	0.411	0.683	0.998	2.842	0.420	0.999	1.644	0.588	0.998

Co-polymer of Acrylamide and Acrylate (HPAM)

Figure 17 shows the percentage ratio of apparent viscosity to initial apparent viscosity of HPAM as a function of time at a shear rate of 20 sec^{-1}. Clear tendencies can be observed even when the data presents some scattering. In the presence of nitrogen, the HPAM polymer solution was able to retain 84% of its original apparent viscosity after 215 days at reservoir temperature of 122 °F. After one day of aging, the apparent viscosity increased to 140% of its initial value. We attribute this increment to a crosslinking effect due to the fast kinetics of the reaction at 122 ºF. Low concentrations of ferric or ferrous ions, in the order of 10 mg/L, can result in the presence of small gels that can increase the apparent viscosity of HPAM solutions (Ramsden and McKay 1986, Yang and Treiber 1985).Chrome compounds form ions that reacts with the hydrolyzed groups in the polymer molecules resulting in the formation of a network or gel. The kinetics of this reaction is within a few hours and also requires low concentrations of chromium, from 5 to 10 mg/L(Jain et al. 2005). The presence of aluminum cause the formation of gel aggregates that also increase solution viscosity, the presence of 10 mg/L was shown by Al-Assi et al. (2009) to increase the viscosity of a solution of 400 mg/L of polyacrylamide in 30% after 1 day. The distilled water used to prepare the solutions was not submitted to further purification by ion exchange or filtration, and therefore contains low concentrations of ions (ASTM 2011). An analysis of a water sample from the same distillation unit used for our investigation revealed the presence of 2.16 mg/L of Al, 1.84 mg/L of Cr, and less than 0.5 mg/L of iron. The presence of these concentrations of Al and Cr can cause partial crosslinking or gel aggregates that can result in the increment of the apparent viscosity to 140% of its initial value.

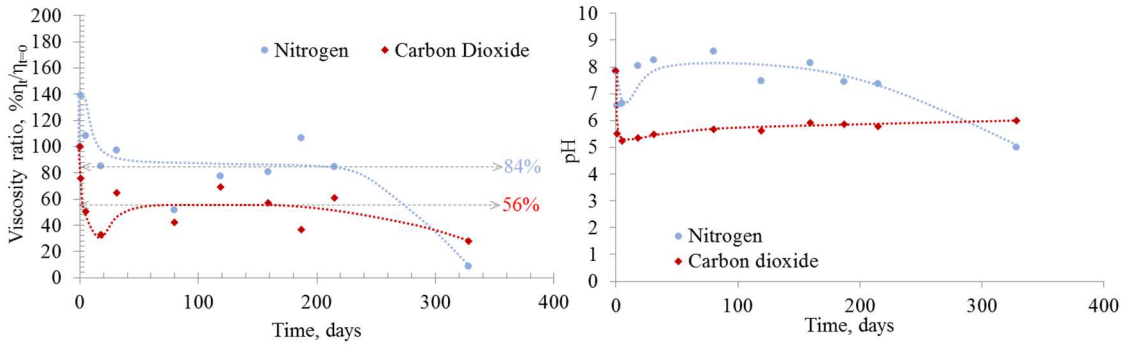

Figure 17. Viscosity retention and pH as a function of time for HPAM solutions aged with nitrogen or carbon dioxide. Temperature is 122 ºF and shear rate is 20 sec^{-1}.

Following the initial increase in apparent viscosity, the HPAM solution aged in nitrogen dropped its apparent viscosity to approximately 85% of its initial value after 18 days. Even at low concentrations of oxygen, oxidation-reduction reactions occurs between transition ions (Cu^{+}, Cu^{2+}, Fe^{2+}) and products of the photolysis of the polymerization initiator with formation of free radicals that can cause oxidative degradation of the HPAM (Kheradmand, Francois, and Plazanet 1988, Levitt and Pope 2008). After the stoichiometry of the reaction was fulfilled, no further degradation happened and the viscosity was maintained for 215 days.

After 328 days, the HPAM solution aged in the presence of nitrogen lost almost all its viscosity and approached to the behavior of a Newtonian fluid, as denoted by the consistency coefficient (n) in Table 6. The strong degradation of the HPAM solution is the result of the hydrolysis of the amide groups into acrylate groups. At 122 °F, the kinetics of the hydrolysis reaction is very slow, but can cause a deterioration in the solution viscosity at low concentration of divalent cations (< 200 mg/L) over aging for an extended period, even when no precipitation occurs (Ryles 1987). Precipitation was not detected in any of the bottles during the course of our experiments.

The apparent viscosity presented a different behavior for the HPAM aged in the presence of carbon dioxide (Figure 17). A rapid decline occurred soon after the aging process started. After 18 days at 122 °F the

apparent viscosity dropped to approximately 33% of its initial value. Carbon dioxide caused the formation of carbonic acid decreasing the pH close to 5. The presence of an acid influence the viscosity of the HPAM solution due to neutralization of the charges on the polymer particles by transforming the ionic carboxylate groups into non-ionic carboxylic acid groups (Mungan 1969). After that first decrease in apparent viscosity, the hydrolysis of the amide groups resulted in the formation of acrylate groups and the evolution of the ammonium ion (Levitt and Pope 2008, Seright et al. 2010). The kinetics of the hydrolysis reaction increases under acid or basic conditions (Kheradmand, Francois, and Plazanet 1988). Consequently, apparent viscosity and pH increased. After aging for 215 days the HPAM solution was able to retain 56% of its initial apparent viscosity. Similar to the case of aging under the presence of nitrogen, the continued hydrolysis during an extended period at low temperature led to the degradation of the polymer solution by interaction of the acrylate groups with the divalent cations.

Co-polymer of Acrylamide and ATBS (PAM – ATBS)

Figure 18 presents the percentage ratio of apparent viscosity to initial apparent viscosity as a function of time for the solution of PAM-ATBS at a shear rate of 20 sec^{-1} and 122 °F. Similar to the previous case, the rapid increase in apparent viscosity after a few days aging at reservoir temperature is probably due crosslinking effects of iron, chrome and other ions present in the preparation water. Following this, the apparent viscosity increased to approximately 130% of its initial value over an aging period of 215 days. The hydrolysis of the β,β dimethyl taurine from the AMPS group, which also results in the formation of an additional acrylate moiety only occurs at temperatures above 212 °F, resulting in the better performance of this polymer compared to HPAM against chemical degradation (Audibert and Argillier 1995, Levitt and Pope 2008). However, some of the amide groups will hydrolyze and transform into acrylate groups, resulting in a ter-polymer of Acrylamide-Acrylate-AMPS. The interaction of those acrylate groups in the ter-polymer with the divalent cations probably caused a slight drop in apparent viscosity resulting in final apparent viscosity of 124% of the one at initial conditions, after aging for 328 days.

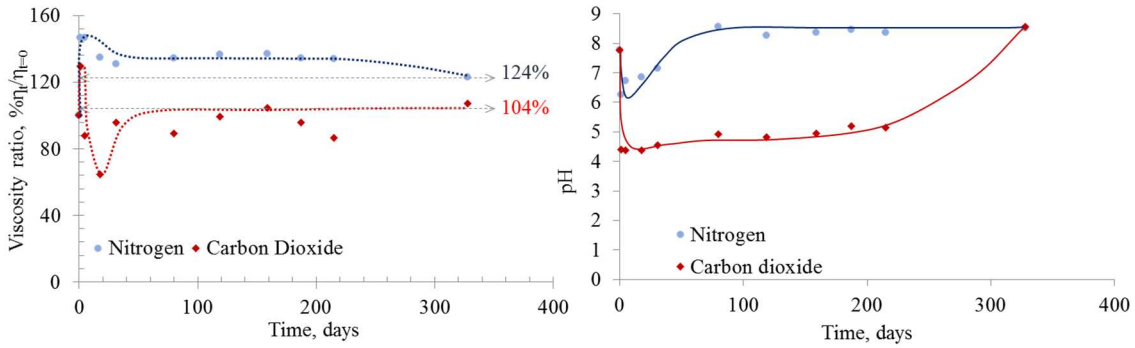

Figure 18. Viscosity retention and pH as a function of time for the PAM-ATBS solutions aged with nitrogen or carbon dioxide. Temperature is 122 ºF and shear rate is 20 sec^{-1}.

For the case of the PAM-ATBS aging in the presence of CO_2, a rapid increase of 30% in apparent viscosity took place after one day at 122 °F. Following that, the reaction of CO_2 and water resulting in carbonic acid decreased the pH and the apparent viscosity. The apparent viscosity recovered, and after 328 aging at reservoir temperature with carbon dioxide present the apparent viscosity of the PAM-ATBS solution was able to increase to 104% of its initial value. The increase in pH over time suggest the evolution of the ammonium ion due to the hydrolysis of the amide groups. The conditions of low pH promoted by the carbonic acid increased the velocity of the hydrolysis reaction.

Effect of Carbon Dioxide

Carbon dioxide caused further degradation in both polymers types. The HPAM solution was able to retain 56% of its original apparent viscosity when aged in the presence of carbon dioxide during 215 days, compared with 84% in an environment saturated with nitrogen. Since the only difference between the samples was the gas inside the bottles, the additional loss of 28% of apparent viscosity is a consequence of the presence of CO_2. This does not mean HPAM cannot be used for chemically assisted CO_2 WAG EOR processes, but proper assessment of the degradation extend have to be performed under the conditions of the particular reservoirs to determine if an increase in HPAM concentration can compensate the degradation

process. The strong degradation observed after 328 of aging cannot be attributed to CO_2 since was also observed for the solution aged in nitrogen.

On the other hand, the PAM-ATBS polymer solution presented excellent performance under the presence of carbon dioxide. Even when CO_2 reduced the increment in apparent viscosity in 20% compared with the solution aged with nitrogen, the polymer solution of PAM-ATBS aged with carbon dioxide increased its apparent viscosity in 4%, reaching 104% of its original apparent viscosity after 328 days aging under reservoir temperature. PAM-ATBS is a good candidate to be used under chemically assisted CO_2 WAG. Both polymers presented an important decrease in apparent viscosity within the first 18 days of aging at reservoir temperature. Even when the viscosity was later recovered, this period of low viscosity can have a detrimental effect in sweep efficiency when the polymer slug contacts the CO_2 slug in the reservoir. To overcome this effect, polymer concentration could be increased to compensate the viscosity loss.

The experiments presented in this thesis were performed under room pressure. The increase in pressure when the solution is injected into the reservoir will lead to an increase in the solubility of CO_2 into water. That effect is neglected in this work. However, the solubility of CO_2 in water has been neglected in other research since is low when compared to the solubility of CO_2 in oil (Valbuena and Barrufet 2013). Another deviation is that CO_2 will be at supercritical state under most reservoir conditions as opposed to vapor state in our experiments, we did not assess the extent of the effect this may have in polymer stability.

MINIMUM MISCIBILITY PRESSURE

Six different runs were performed to experimentally determine the MMP of the dead NBU crude oil – CO_2 system. The results of those experiments are presented in Table 7. Figure 19 shows a plot of recovery factor as a function of test pressure for the MMP experiments. A strong dependency of recovery on pressure is revealed for the points at 500 and 1000 psia. The increment of 500 psia in pressure resulted in an increment of approximately 30 % in recovery. This behavior suggest that increasing the pressure leads to lower

capillary forces retaining the crude in the porous media as a consequence of lower interfacial tension (IFT) in the oil – CO_2 interface. The reduction of the IFT as pressure increases is a consequence of an increment in the dissolution of CO_2 into the oil, and the vaporization of hydrocarbon components into the CO_2. The mass exchange between CO_2 and the crude oil could be only improved in that proportion if they remain as two different phases, and therefore, in that region of the plot miscibility has not been achieved.

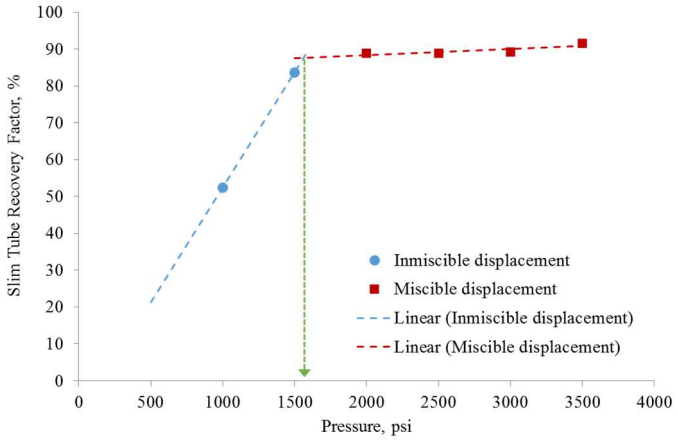

Figure 19. Recovery factor as a function of pressure for the MMP determination of the system NBU crude oil - CO_2

On the other hand, between 2000 and 3500 psia the increment in recovery is negligible. This indicates that further improvement in displacement efficiency is difficult. This can only happen when there is no longer an interphase separating CO_2 and crude oil, and they are mixed in all proportions leading to displacement efficiency close to the unity. Therefore, that region of the plot is regarded as the miscible region. The minimum miscibility pressure of the system dead NBU crude oil and CO_2 is the pressure at which the extrapolation of the lines corresponding to the immiscible and miscible portions of the plot intersect each other.

Table 7. Test pressure and oil recovery for the determination of MMP of the NBU crude oil/CO_2 system

Test pressure, psia	*Oil recovery, % of OOIP*
1000	52.43
1500	83.61
2000	88.81
2500	88.81
3000	89.26
3500	91.59

A MMP of 1563 psia was found from the data plotted by fitting the equation of a line to each one of the regions, miscible and immiscible, and solving simultaneously for the pressure at which recovery is the same in both equations. The MMP obtained is close to previously reported MMP from slim tube of 1687 psia, measured using recombined oil of the same field in a 40 ft column (CoreLab 2010). It is also similar to the MMP value of 1680 psia calculated with the Peng-Robinson equation of state (EOS) using a fluid model based on a PVT analysis from the NBU (Li et al. 2014). The oil sample used is not the same as used in the previous experimental determination, neither the column length and experimental protocol and therefore slightly different values are not surprising (Ekundayo and Ghedan 2013). Also, solution gas can have an effect in MMP. Our study was performed using dead oil, whereas previous MMP studies were performed for an oil sample recombined at a ratio of 20 scf/bbl. Experimental results derived from MMP determinations using the raising bubble apparatus (RBA) indicate that MMP decreases as solution gas decreases (Dong, Huang, and Srivastava 2000).

As it was detailed during the experimental procedure, the column used for the MMP experiments was particularly short. The length of our column was only 20 ft as opposed to the traditional columns whose lengths usually range from 40 to 80 ft. This change had a positive effect since the time employed for each displacement was considerable reduced. However, the accuracy of the results was somehow compromised. The pore volume of the column employed was only approximately 20 ml. Similar to the dead volume of the displacement equipment. This situation makes our equipment more susceptible to errors, as a measurement error of 1 ml in the oil production would translate into an error of 5% in the calculated recovery factor.

Therefore, even when the dead volume of the equipment was estimated using two different approaches for verification purposes, it is believed that the error in this magnitude is responsible for the low values of recovery, around 90%, obtained under miscible displacements. The recovery factor during slim tube experiments when miscibility is reached is usually close to 100%.

CORE FLOODING EXPERIMENTS

Homogeneous Rock, Immiscible Displacement

The homogeneous rock displacements under immiscible conditions were performed in Bentheimer cores at 1300 psia, below the estimated MMP of 1563 psia. Table 8 summarizes the results. All the cores in this section had similar dimensions of 2 in of diameter and 6 in of length. Since porosity was also very similar (Figure 20), the pore volume was comparable.

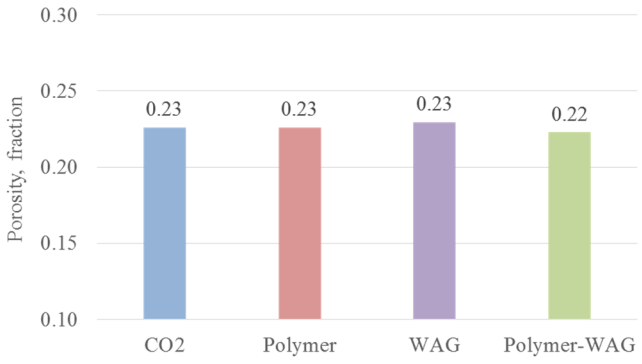

Figure 20. Porosity of the Bentheimer homogeneous core plugs used for the immiscible displacements. Runs 1.1 to 1.4 are presented.

Table 8. Summary of results for the core flooding experiments performed in homogeneous Bentheimer sandstone under immiscible displacement conditions

	CO_2	*Polymer*	*WAG*	*Polymer-WAG*
Run ID	1.1	1.2	1.3	1.4
Porosity, fraction	0.23	0.23	0.23	0.22
Pore volume, cm^3	69.82	69.82	70.82	68.82
Permeability, k, Darcy	1.604	1.521	1.627	1.468
OOIP, cm^3	44.15	45.15	44.15	49.15
RF_{water}, % of OOIP	31.06	34.80	28.79	38.07
RF_{EOR}, % of OOIP	18.12	5.54	24.92	22.38
RF_{Final}, % of OOIP	49.18	40.34	53.71	60.45
S_{wi}, fraction	36.77	35.34	37.67	28.59
S_{oi}, fraction	63.23	64.66	62.33	71.41
$S_{or\ water}$, fraction	43.59	42.16	44.39	44.22
$S_{or\ EOR}$, fraction	32.13	38.58	28.86	28.24

Rock absolute permeability is also parallel. The slopes of the curves in Figure 21 represent the absolute permeability to the injected reservoir brine prepared in the laboratory. The good alignment of the points reveal consistency in the measurement of absolute permeability. Only the run 1.4, corresponding to the polymer assisted WAG case deviates from the general trend. As mentioned during the description of the procedure, different core plugs were used for each one of these runs and therefore the rock properties are expected to be similar, but not identical.

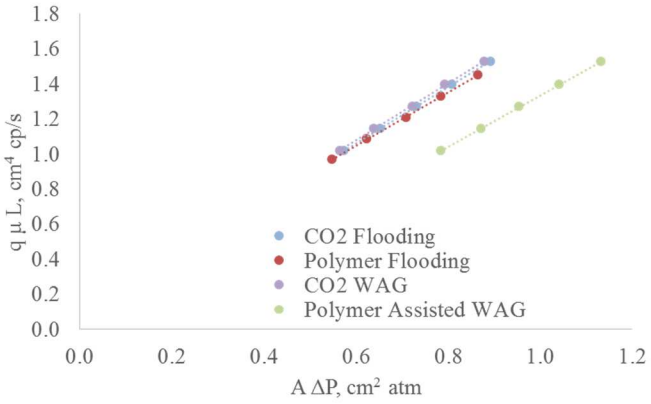

Figure 21. Absolute permeability comparison for the core flooding tests in homogeneous Bentheimer core plugs under immiscible displacement conditions

During the stage of oil injection, the water saturation was reduced to the initial water saturation value (S_{wi}). The run 1.4, corresponding to the polymer assisted WAG case, deviates one more time of the general behavior as more water was displaced, leading to a higher OOIP and a lower S_{wi}. The rest of the runs present comparable values of both OOIP and S_{wi}. During the water flooding process, the recovery factor reached for the polymer assisted WAG (run 1.4) was also different than for the rest of the runs. In this case, water injection led to higher recovery, compensating for the higher value of OOIP and resulting in similar residual oil saturations ($S_{or\ water}$) after water flooding for all the runs.

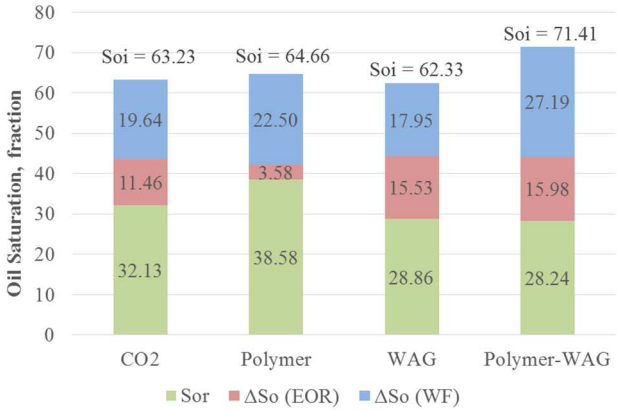

Figure 22. Initial oil saturation, oil saturation change due to water flooding and EOR and residual oil saturation for the immiscible displacements in homogeneous Bentheimer cores

The EOR stage was then started at similar conditions of residual oil saturation after water flooding ($S_{or\ water}$) for all the runs presented in this section. The injection of 1 PV of CO_2 below MMP recovered an additional 18.12 % of the OOIP and led to a final residual oil saturation ($S_{or\ EOR}$) of 32.13 %, meaning that caused a reduction of 11.46% in residual oil saturation (Figure 22). Immiscible CO_2 flooding is an effective EOR process under this conditions as oil swelling and viscosity reduction are active recovery mechanisms. On the other hand, the polymer flooding performance was poor. The injection of 1 PV of polymer only led to an incremental oil recovery of 5.54 % of OOIP, causing a reduction of only 3.58 % in oil saturation after

water flooding. This result is not surprising as polymer is focused in improving sweep efficiency and mobility control, and mobility problems are more important in heterogeneous rocks.

The implementation of a WAG scheme led to higher recovery compared to the continuous CO_2 injection case. The injection of CO_2 - WAG (run 1.3) increased recovery in 24.92 % of OOIP over water flooding and caused a reduction of 15.53% in oil saturation. The final residual oil saturation ($S_{or\ EOR}$) in the Bentheimer core plug used was 28.86%, which is lower than the 32.13 % of $S_{or\ EOR}$ observed after continuous CO_2 flooding. This is an indication that immiscible CO_2 flooding suffers from a mobility control problem that can be mitigated by the use of a WAG process.

The addition of water soluble polymers during WAG did not improved the process. The final $S_{or\ EOR}$ reached after the injection of the polymer assisted WAG EOR scheme was 28.24%, only slightly lower than the 28.86% gotten by the conventional WAG. This is consistent with the results shown for the polymer flooding run. The role of the polymer is to improve sweep efficiency of the water, causing water to contact more rock volume in the core. The mobility ratio during the water flooding was 16 and the polymer injection was designed to reduce such mobility ratio to the unity. Our results indicate that an adverse mobility ratio of 16 in a water flooding process, in the absence of significant heterogeneities does not justify the use of a polymer as the benefit is not noteworthy.

The oil saturation as a function of cumulative injection is presented in Figure 23. An interesting behavior is observed for the continuous CO_2 injection as the oil recovery during the EOR phase is perceived during the chase water stage (final dark blue line) instead of during the actual CO_2 injection (light blue center line). An explanation for this is the severely adverse mobility ratio between CO_2 and oil that caused the CO_2 to finger through the oil without displacing any significant oil volume. The viscosity of CO_2 at 122 °F and 1300 psia is 0.023 cp. But as the injection progressed the oil was swelled and its viscosity was reduced by the presence of CO_2 allowing the chase water to displace it outside of the core. It is necessary to point out that even when the chase water is intended to displace the injected CO_2 and the oil bank outside the core holder, since 1 PV

of CO_2 was injected and not all the oil and water inside the core can be displaced by the CO_2, breakthrough of CO_2 is expected before the CO_2 injection finish and some oil production is also anticipated.

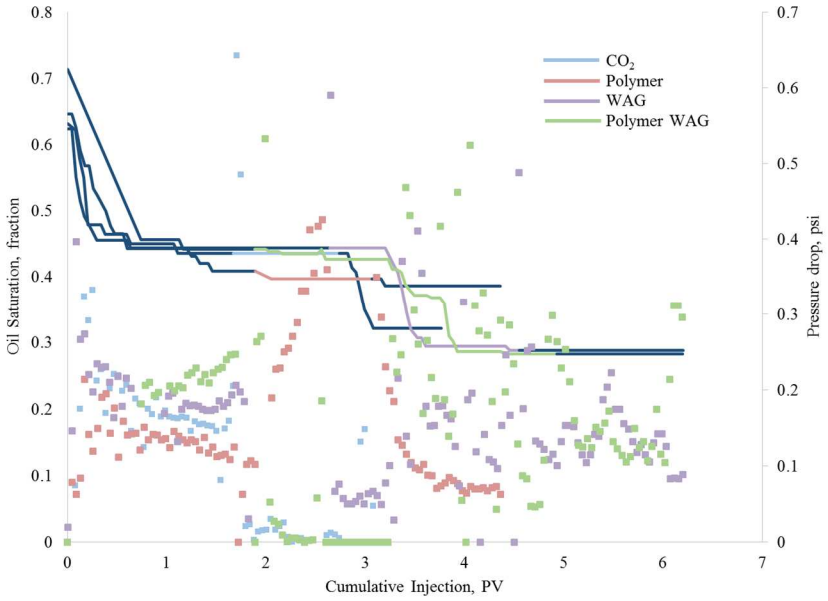

Figure 23. Oil saturation and pressure drop as a function of cumulative injection for the homogeneous Bentheimer cores under immiscible displacement. The lines are oil saturation and the dots are pressure drop. The dark blue lines correspond to water flooding and chase water. The colored line correspond to the EOR stage. The pressure drop are in the same color as their corresponding EOR stage.

The pressure drop as a function of injected volume can be also observed in Figure 23. The pressure points are coded with the same colors as the oil saturation. The plot reveals the effectiveness of the polymer in increasing viscous forces as the pressure drop recorded during polymer flooding (pink points) and during polymer WAG (green points) are larger than the ones recorded for carbon dioxide (light blue) and conventional WAG (purple). The pressure drop during polymer flooding presents the highest values as once the polymer has breakthrough at the producing end of the core holder, it is mainly polymer what is flowing through the core, and the pressure drop will increase according to the viscosity increase. For the polymer WAG case, the pressures are lower since only small slugs of polymer are injected and those slugs flow

together with CO_2 slugs. The purple points reveal the improvement in mobility caused by the use of the WAG scheme as the pressure drop is higher than in the CO_2 case.

Homogeneous Rock, Miscible Displacement

The homogeneous rock displacements under miscible conditions were performed in Bentheimer sandstone core plugs at 1850 psia, above the MMP pressure determined during the slim tube experiments of 1563 psia. Table 9 shows a summary of all the results. The porosity of the cores is similar (Figure 24), and since all of the Bentheimer core plugs had the same dimensions of 2 in of diameter and 6 in of length, the pore volumes are comparable.

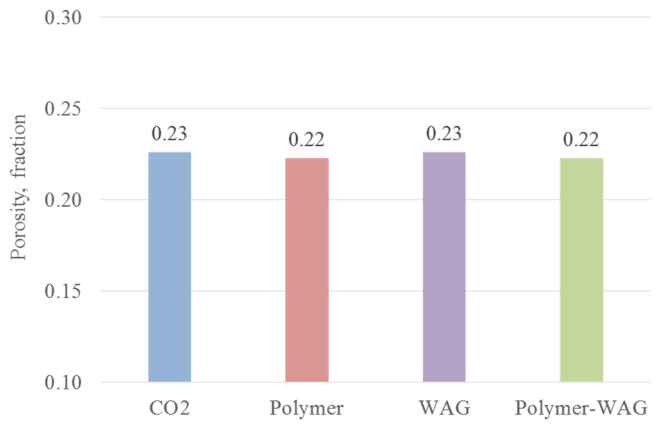

Figure 24. Porosity of the Bentheimer homogeneous core plugs used for the miscible displacements. Runs 2.1 to 2.4 are presented.

The absolute permeability was carefully determined and the good alignment of the points in Figure 25 shows the consistency of the measurement. The slope of the curves in Figure 25 correspond to the values of absolute permeability presented in Table 9. For these runs the core plugs are not as similar among each other in terms of permeability as for the immiscible case. The absolute permeability ranges from 0.963 Darcy to 1.299

Darcy. Nevertheless, as the percent difference between those values is not large, we do not expect this variation to have a profound impact in the displacement process.

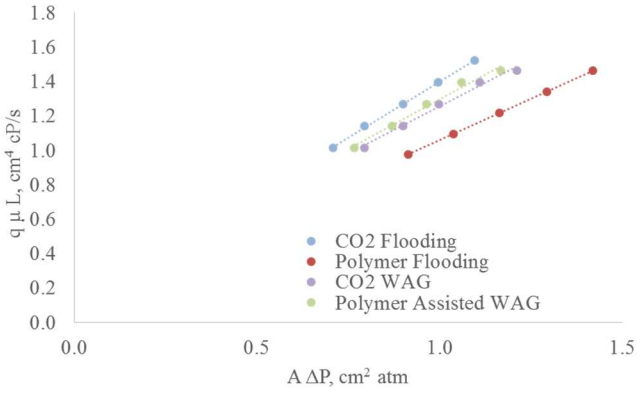

Figure 25. Absolute permeability comparison for the core flooding tests in homogeneous Bentheimer core plugs under miscible displacement conditions

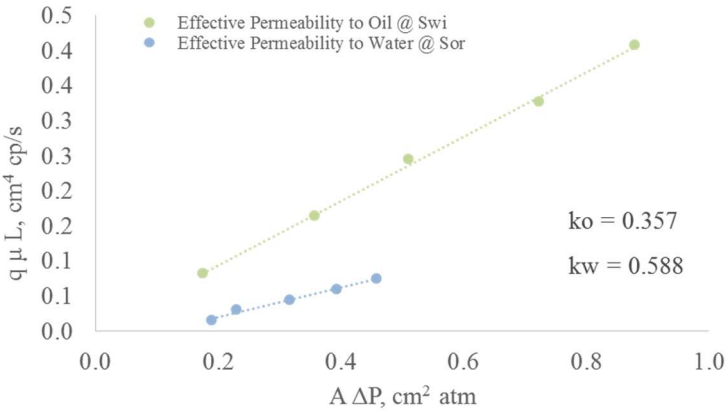

Figure 26. Effective permeability to oil and water for core flood 2.2

The polymer flooding run (run 2.2) was selected to estimate the effective permeability to oil and water used for the estimation of polymer concentration. The slopes in Figure 26 corresponds to an effective permeability

to oil of 0.357 Darcy and to water of 0.588 Darcy. In the same manner as for the absolute permeability case, the good alignment of the curves indicate the consistency of the measurement, as the increment in the pressure drop is proportional to the increment in the injection rate, following Darcy equation (Eq. 9).

Table 9. Summary of results for the core flooding experiments performed in homogeneous Bentheimer sandstone under miscible displacement conditions

	CO_2	*Polymer*	*WAG*	*Polymer-WAG*
Run ID	2.1	2.2	2.3	2.4
Porosity, fraction	0.23	0.22	0.23	0.22
Pore volume, cm^3	69.82	68.82	69.82	68.82
Permeability, k, Darcy	1.299	0.963	1.099	1.154
OOIP, cm^3	48.15	47.15	46.15	47.15
RF_{water}, % of OOIP	36.78	39.68	31.88	31.20
RF_{EOR}, % of OOIP	54.00	2.12	43.99	31.82
RF_{Final}, % of OOIP	90.78	41.81	75.87	63.02
S_{wi}, fraction	31.04	31.50	33.91	31.50
S_{oi}, fraction	68.96	68.50	66.09	68.50
$S_{or\ water}$, fraction	43.59	41.32	45.05	47.13
$S_{or\ EOR}$, fraction	6.35	39.87	15.95	25.34

The synthetic reservoir water displacement by oil resulted in similar OOIP and S_{wi} for all the homogeneous rock experiments under miscible conditions. The highest deviation is presented by the case of conventional WAG which had the lowest OOIP, 46.15 cm^3 and therefore the highest S_{wi} of 33.91%. The water flooding stage presented different results for all the tests. The highest recovery during water flooding was presented by the run for the polymer flooding, with a recovery factor of 39.68% of OOIP. This was followed by the run for the continuous CO_2 injection, where water injection yielded a recovery factor of 36.78%. The water flooding recovery for the remaining two runs were similar, close to 31 %. The reasons for such difference is unknown, as there is not a direct correlation with the permeability values that could be tied to capillary forces.

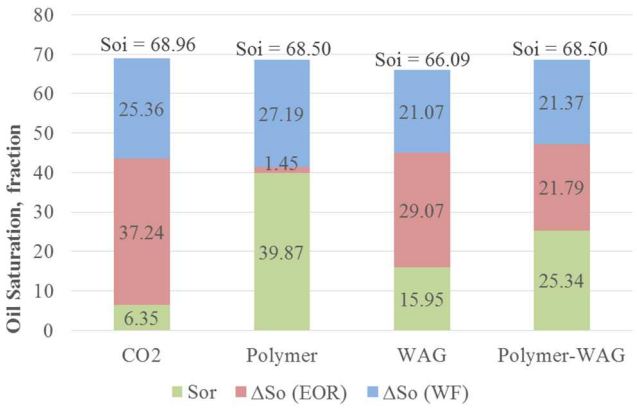

Figure 27 Initial oil saturation, oil saturation change due to water flooding and EOR and residual oil saturation for the homogeneous Bentheimer cores under miscible conditions

The EOR stage for the miscible runs yielded interesting results. The continuous injection of CO_2 resulted in a very high incremental oil recovery of 54 % of OOIP, leading to an ultimate recovery for this run of 90.78%. The injection of carbon dioxide above MMP reduced the oil saturation from 43.59 % to as low as 6.35 % (Figure 27). The high performance of CO_2 is a consequence of the absence of an interface, as miscibility is reached, leading to a suppression of the capillary forces acting in the porous media. Even in a supercritical state, the viscosity of CO_2 is very low (0.048 cp at 122 °F and 1850 psia), and therefore, viscous fingering is expected. However, as a consequence of the fast molecular diffusion related to the miscibility between the phases, and the low advance rate of 1 ft/day used during our experiments is believed that any viscous fingering occurring at the front was dispersed.

Similarly than in the run at 1300 psia, the incremental recovery with polymer at 1850 psia was poor. In this case, 3.5 PV of polymer were injected to make sure that adsorption of polymer on the rock surface reached equilibrium. The same reasons that caused the poor performance at 1300 psia hold true in this case, as neither water or polymer viscosity are severely affected by the pressure increase. The oil viscosity is not considerable affected either since dead oil is being used.

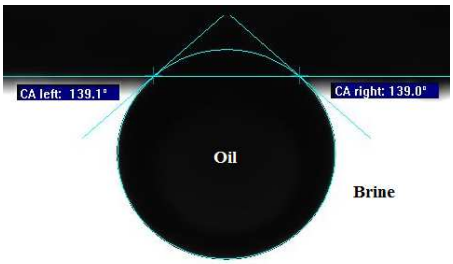

Figure 28. Contact angle measurement using the captive drop technique for the Bentheimer rock. The rock is strongly water wet.

When the WAG process was implemented, an incremental recovery factor over water flooding of 43.99 % of OOIP was achieved. And the final oil saturation ($S_{or\ EOR}$) remaining in the core was 15.95. The implementation of WAG had a detrimental effect over recovery when compared to the miscible continuous CO_2 flooding, where the residual oil saturation ($S_{o\ EOR}$) was reduced to 6.35%. The reason for this response is that the mobile water injected shielded some of the oil drops from being reached by the CO_2. This phenomena has been studied by different authors and it has been found to be more severe in strongly water wet rocks (Stalkup 1970). Figure 28 shows the result of the contact angle measurement on Bentheimer sandstone using the captive drop method in a pendant drop contact angle device. The angle of 139° and 139.1° measured in both sides inside the oil drop reveals the water wet condition of the Bentheimer rock (Anderson 1986), and supports the water shielding theory.

The addition of water soluble polymer to the WAG scheme it is believed to have worsened the water shielding phenomena. This run exhibited lower recovery in the EOR stage than both continuous CO_2 flooding and conventional tapered WAG. The incremental oil recovery was only 31.82% of OOIP over water flooding and the oil saturation ($S_{or\,EOR}$) was reduced to 25.34 %. Much more than the 15.95 % achieved by WAG, and the 6.35 % of CO_2 flooding, meaning that more oil was left behind. A potential justification for this detrimental effect is that as the polymer increased the water viscosity, water was able to contact

more reservoir rock preventing more oil to be contacted by the CO_2. Since the CO_2 and water are not miscible the first is unable to effectively diffuse through the second to reach the oil surrounded by the polymeric solution, and therefore, is unable to displace it.

The oil saturation and the pressure drop as a function of cumulative injection is shown in Figure 29. The pressure drop is considerably higher during the polymer injection, which indicates that viscous forces where increased by the presence of the polymer. Similarly, the polymer assisted WAG run presented higher pressure drop values when compared with the CO_2 injection and the conventional WAG.

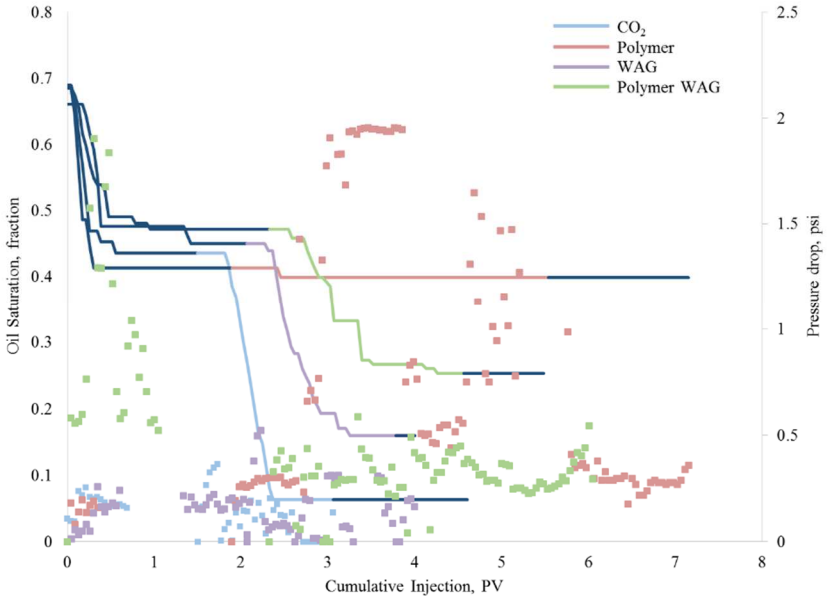

Figure 29. Oil saturation and pressure drop as a function of cumulative injection for the homogeneous Bentheimer cores under miscible displacement. The lines are oil saturation and the dots are pressure drop. The dark blue lines correspond to water flooding and chase water. The colored line correspond to the EOR stage. The pressure drop are in the same color as their corresponding EOR stage.

Heterogeneous Rock, Immiscible Displacement

The core flooding tests for heterogeneous rock were performed using a composite core built with two actual NBU core plugs selected from the vertical well NBU 4828 in the North Burbank Unit, Oklahoma. Only two runs were performed, to compare immiscible WAG, with immiscible polymer assisted WAG. A summary with the results of the two experiments is presented in Table 10. As opposite to the homogeneous case, where a different Bentheimer core plug was utilized for each run, both experiments were performed in the same composite core plug. After run 3.3 was finished, the two core pieces comprising the composite core plug were cleaned using toluene in a Dean-Stark set up (Dean and Stark 1920).

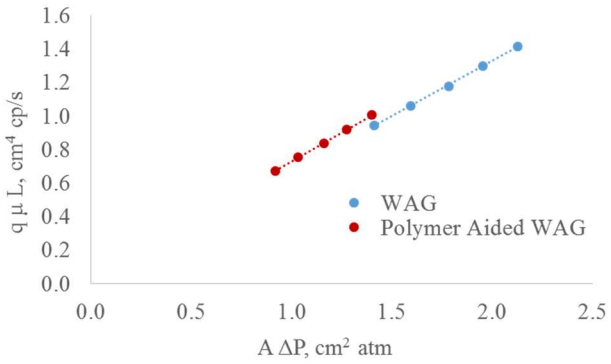

Figure 30. Absolute permeability for both runs in the heterogeneous NBU composite core under immiscible conditions

However, due to the brittle nature of the NBU reservoir rock, both core plugs were fractured at their ends during the extraction from the core holder. Consequently, the cores where reshaped before they were packed again for the test 3.4, resulting in different core length in each test. Despite this change in the composite core, the porosity measured in both cases was the same, however, the resulting pore volume is different. Similarly, the absolute permeability remained almost unchanged (Table 10). The slopes in Figure 30 correspond to the permeabilities shown in Table 10. Both slopes are comparable even when the points are

shifted as a consequence of the change in the length of the individual pieces of the composite core plug. The alignment of the points show the consistency of the absolute permeability measurement.

Table 10. Summary of results for the core flooding experiments performed in heterogeneous NBU sandstone under immiscible displacement conditions

	WAG	*Polymer-WAG*
Run ID	3.3	3.4
Porosity, fraction	0.25	0.25
Pore volume, cm^3	76.82	55.82
Permeability, k, Darcy	658	697
OOIP, cm^3	42.15	22.04
RF_{water}, % of OOIP	6.43	9.26
RF_{EOR}, % of OOIP	51.96	34.03
RF_{Final}, % of OOIP	58.39	43.28
S_{wi}, fraction	45.14	60.52
S_{oi}, fraction	54.86	39.49
$S_{or\ water}$, fraction	51.33	35.83
$S_{or\ EOR}$, fraction	22.83	22.39

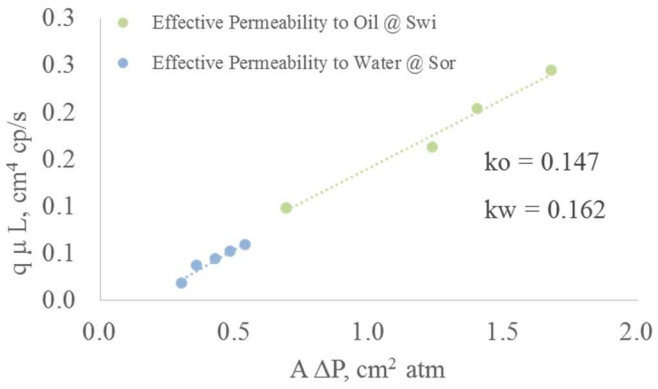

Figure 31. Experimental results for the determination of effective permeability to oil and water in the NBU rock.

The effective permeability to oil and water for the polymer concentration estimation were measured in this core sample. The slopes in Figure 31 correspond to an effective permeability to oil of 0.147 Darcy and an effective permeability to water of 0.162 Darcy. The alignment of the points is not as good for this case as for the previous cases since the stabilization of the pressure drop was difficult as a consequence of the low effective permeability values, but enough time was given to reach steady state conditions and obtain measurements with acceptable consistency.

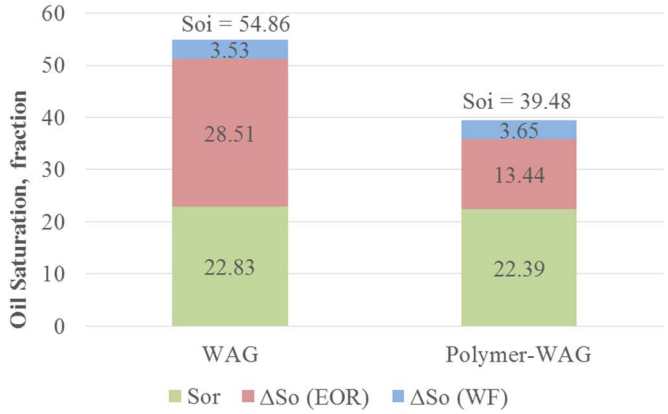

Figure 32. Initial oil saturation, oil saturation change due to water flooding and EOR and residual oil saturation for the heterogeneous NBU core plug under immiscible conditions

The displacement of the synthetic reservoir brine by the dead crude oil from the NBU yielded different distributions for initial oil (S_{oi}) and water (S_{wi}) saturations. The conventional WAG run had higher initial oil saturation (54.86%) than the polymer assisted WAG experiment (39.49 %). The water flooding recovery was low, and reduced the oil saturation only in about 3.5 % in both cases (Figure 32). The low recovery under water flooding is justified by the intermediate wettability condition of the reservoir rock (Figure 33). The differences in the initial distributions of saturations, and the similar behavior of water flooding resulted in different residual oil saturations after the water injection was completed.

The oil saturation ($S_{or\ water}$) was 51.33% at the beginning of the conventional WAG injection in run 3.3, and 35.83 % at the beginning of the polymer assisted WAG run. This condition makes difficult the comparison of the experiments since the conventional WAG has the advantage of a higher volume of oil available to be mobilized. The incremental recovery factor under conventional WAG was 51.96 % of OOIP over water flooding, which is considerably higher than the one obtained by the polymer assisted WAG, of 34.03 % of OOIP (Table 10). However, the residual saturation of oil achieved by both methods is comparable (Figure 32), and this is an indication that the addition of polymer to the water during WAG in heterogeneous NBU rock did not benefit the process in terms of recovery, but it was not detrimental either.

When compared with the homogeneous experiments presented in the earlier sections (Table 8 and Table 9), the initial water saturation (S_{wi}) was higher for both heterogeneous cases. This can be a result of the lower permeability observed in the NBU cores, and the wider grain size distribution that could be expected in rocks with this level of heterogeneity. Both conditions can be related to higher capillary forces inside the porous media. The water flooding recovery was also lower in the heterogeneous case than for the homogeneous runs. The reason for this is that wettability in this case is intermediate (Figure 33), as opposed to the Bentheimer cores which are water wet (Figure 28).

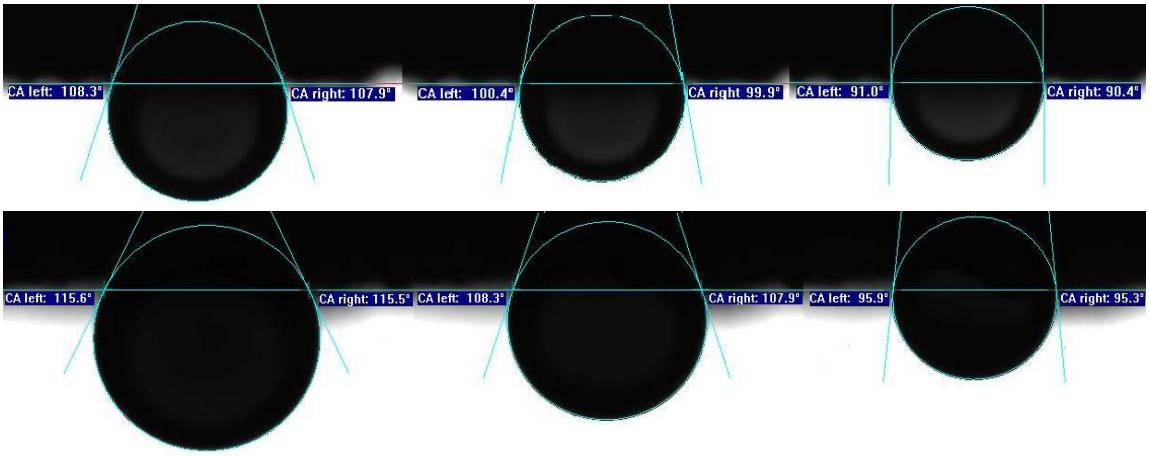

Figure 33. Contact angle measurements for two different samples (above and below) of NBU rock from the well NBU 4828. The images show a neutrally wet surface. The contact angle changed with time, the first contact measurement is located to the left and later the drop shape changed as shown to the right.

Oil saturation and pressure drop over length as a function of injected volume for both immiscible WAG and immiscible polymer assisted WAG are shown in Figure 34. For this case, since the core plug length was reduced after run 3.3, the pressure drop was divided by the core length in each case, and therefore, pressure drop per unit of length is presented to allow for comparison. The pressure drop for the polymer assisted WAG is higher than for the case of the conventional WAG, but the difference is subtle. Capturing the increase in pressure drop due to the presence of the polymer during WAG processes is complicated because there is also CO_2, oil, and water remaining from the previous water flooding present in the porous media, and additionally, their saturations are changing. The dotted line in the plot, indicates a portion of data that was lost due to an energy outage during the course of the experiment, and the change in saturation has been approximated to connect the known points of initial oil saturation (S_{oi}) and residual oil saturation after water flooding ($S_{or\ water}$).

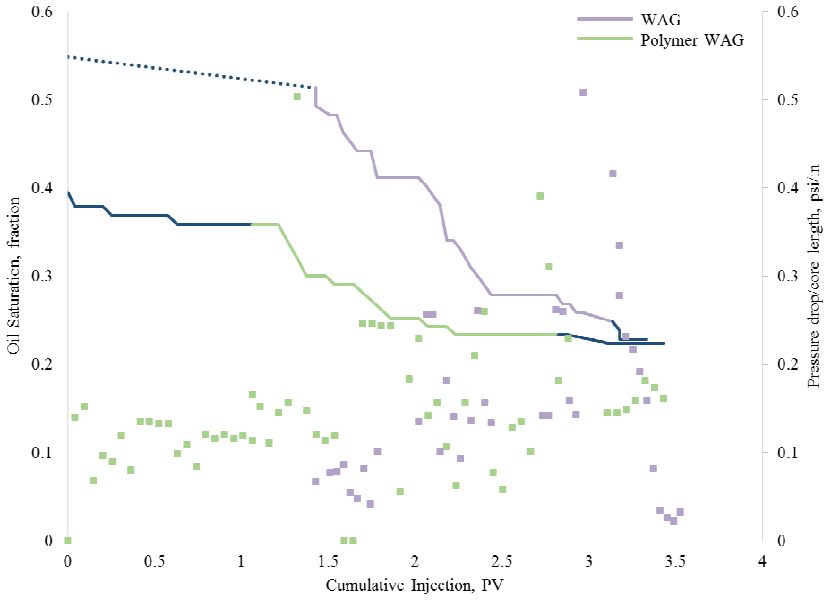

Figure 34. Oil saturation and pressure drop over length as a function of cumulative injection for the core flooding tests in heterogeneous NBU rock under immiscible displacement. The lines are oil saturation and the dots are pressure drop. The dark blue lines correspond to water flooding and chase water. The colored lines correspond to the EOR stage. The pressure drop are in the same color as their corresponding EOR stage.

Heterogeneous Rock, Miscible Displacement

The miscible displacements in heterogeneous rock were performed using a composite core comprised by two core plugs extracted from the well NBU 4828 located in the North Burbank Unit, Oklahoma. Two experiments were carried out, one using a conventional tapered WAG injection scheme and another using polymer assisted WAG. The results for both experiments are presented in Table 11. The same composite core built with the core plugs NBU 4828 -3 and NBU 4828 – 4 was used in both runs. Between experiments, the composite core was cleaned using toluene in a Dean- Stark set up (Dean and Stark 1920).The porosity of the composite core was closely reproduced during the two experiments and therefore the pore volume is comparable.

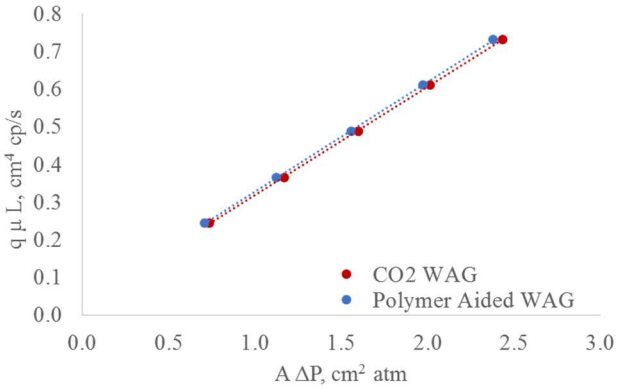

Figure 35. Experimental data for the determination of absolute permeability in runs 4.3 and 4.4.

Absolute permeability was measured under steady state conditions using reservoir brine synthetically reproduced in the laboratory. The slopes in Figure 35 correspond to the absolute permeability for runs 4.3 and 4.4 found in Table 11. The curves in the figure are almost superimposed demonstrating that the absolute permeability was reproduced in both experiments. The alignment of the points expose the consistency of the

permeability measurement as the pressure drop change proportionally to the injection rate according to Darcy equation (Eq. 9).

Table 11. Summary of results for the core flooding experiments performed in heterogeneous NBU sandstone under miscible displacement conditions

	WAG	*Polymer-WAG*
Run ID	4.3	4.4
Porosity, fraction	0.25	0.25
Pore volume, cm^3	70.82	68.82
Permeability, k, Darcy	304.3	311.9
OOIP, cm^3	36.15	33.15
RF_{water}, % of OOIP	10.26	5.16
RF_{EOR}, % of OOIP	68.33	66.37
RF_{Final}, % of OOIP	78.60	71.53
S_{wi}, fraction	48.96	51.84
S_{oi}, fraction	51.04	48.16
$S_{or\ water}$, fraction	45.80	45.68
$S_{or\ EOR}$, fraction	10.92	13.71

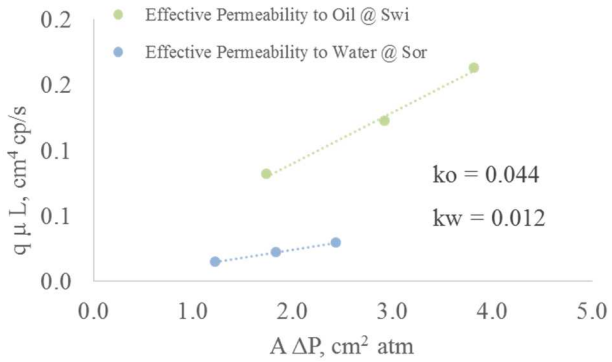

Figure 36. Experimental data for effective permeability to oil and water determination for the core flooding tests in heterogeneous rock at miscible conditions

The effective permeability to oil (k_o) at initial water saturation (S_{wi}), and the effective permeability to water (k_w) at residual oil saturation (S_{or}) were also measured in this composite core. The slope of the curves in

Figure 36 correspond to an effective permeability to oil of 0.044 Darcy and an effective permeability to water of 0.012 Darcy. Those values were used to verify that polymer concentration required to achieve mobility control in this test was not larger than 400 mg/L.

The displacement of the synthetic reservoir brine by the dead NBU crude oil yielded similar initial water (S_{wi}) and oil (S_{oi}) saturations for both experiments (Table 11). The water flooding stage compensated the small difference between the initial oil saturations (S_{oi}) and therefore the EOR stage was initiated in both experiments with a residual oil saturation after water flooding ($S_{or\ water}$) of 45.8 % for the run 4.3 corresponding to the conventional WAG process, and 45.68% for the run 4.4 corresponding to the polymer assisted WAG. The EOR stage also yielded similar results, the use of a tapered WAG scheme was able to reduce the oil saturation in 34.88 % to achieve a final residual oil saturation ($S_{or\ EOR}$) of 10.92 %. Whereas the implementation of polymer assisted WAG resulted in an oil saturation decline of 31.97 % reaching a final residual oil saturation ($S_{or\ EOR}$) of 13.71% (Figure 37).

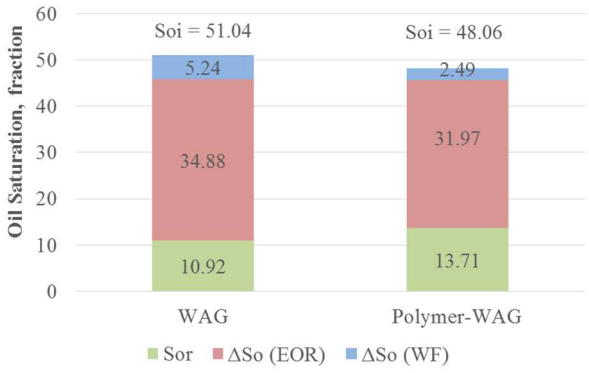

Figure 37. Initial oil saturation, oil saturation change due to water flooding and EOR and residual oil saturation for the heterogeneous NBU core plug under miscible conditions

The performance of the conventional WAG, once again seems to be better than the one for polymer assisted WAG. However, if we compare the results with the ones obtained in the homogeneous cores, it is evident

that the presence of heterogeneities improve the response of the polymer assisted WAG with respect to the response of the conventional WAG, as the gap between their performance, expressed in terms of the final residual oil saturation ($S_{or\ EOR}$) reached was greatly reduced (Figure 27 and Figure 37). This indicates that as the heterogeneities appear, the performance of the miscible carbon dioxide is reduced and the one of the polymer is increased. A discussion about this subject is presented later.

The oil saturation and the pressure drop as a function of injected volume for both miscible WAG and miscible polymer assisted WAG are presented in Figure 38. The pressure drop for the polymer assisted case raises to higher values during the polymer injection cycles when compared with the water injection cycles of the conventional WAG. This is an indication of the increase in viscous displacement forces triggered by the presence of the polymer.

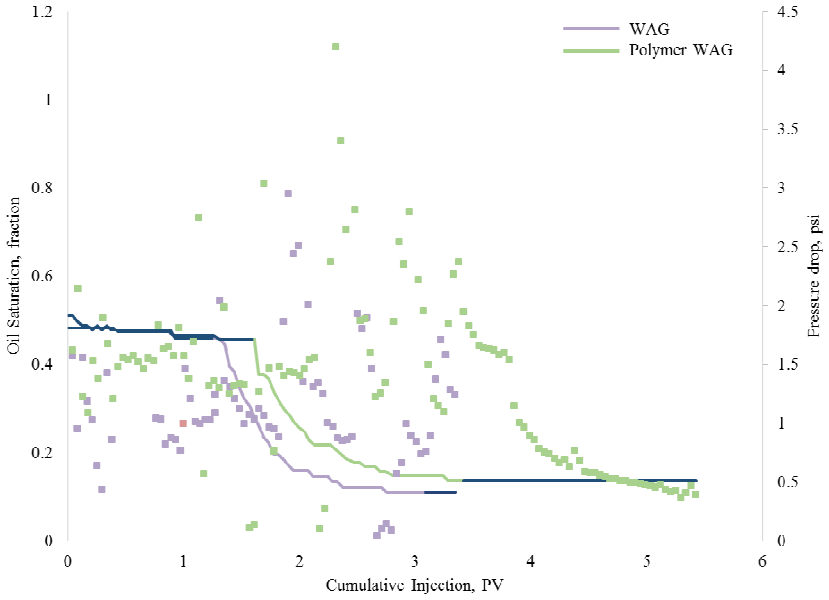

Figure 38. Oil saturation and pressure drop as a function of cumulative injection for the core flooding tests in heterogeneous NBU rock under miscible displacement. The lines are oil saturation and the dots are pressure drop. The dark blue lines correspond to water flooding and chase water. The colored lines correspond to the EOR stage. The pressure drop are in the same color as their corresponding EOR stage.

FURTHER DISCUSSION ON THE USE OF WATER SOLUBLE POLYACRYLAMIDES AS THICKENERS DURING CO_2 WAG EOR AND RECOMMENDATIONS FOR FUTURE WORK

The core flooding experiments have revealed the simultaneous influence of miscibility, viscous fingering, rock heterogeneity and viscosity of the fluids over the final recovery obtained in a WAG process. In the following discussion, we will combine the outcomes from the different core flooding experiments to provide some insights about the dynamics of the WAG process and the effect of the addition of water soluble polymers.

Let us first consider the continuous immiscible CO_2 flooding case in a homogeneous reservoir. Under those conditions it has been shown that viscous fingering of the gas into the oil would reduce ultimate recovery. This was evidenced because implementing WAG under immiscible conditions yielded larger recovery than the continuous immiscible CO_2 flooding, meaning that the mobility control provided by the WAG scheme was positive for the sweep efficiency. We did not perform a continuous immiscible CO_2 flooding in heterogeneous rock, but the heterogeneities can only exacerbate the viscous fingering problem, and therefore, we can be certain that a conventional WAG is beneficial under immiscible conditions. Now, let us consider the addition of the water soluble polymers to the system. In our experiments, both in homogeneous and heterogeneous cores, the addition of the polymer did not cause any meaningful effect. Therefore, it is very improbable that the polymer could be detrimental to the process. However, so far we cannot say either that it is beneficial.

On the other hand, the continuous miscible CO_2 flooding in homogeneous cores recovered almost all of the oil. It is believed that at the low advance rate of the flood the diffusive phenomena induced by the miscibility was fast enough to disperse any possible viscous fingering. When we performed WAG in the miscible homogeneous rock the presence of water was detrimental to the process as it acted like a barrier preventing the CO_2 from contacting some of the oil. The addition of the polymer made the process worse, indicating that water had better sweep efficiency when it was thickened as it was able to reach, and shield, more oil.

Between the ultimate residual oil saturation for the miscible WAG and the miscible polymer aided WAG in the homogeneous rock there was a gap of about 10 %. However, no such difference existed when the heterogeneities were introduced. There are two possible causes for this, the presence of heterogeneities and the less water wet nature of the heterogeneous reservoir rock compared to the homogeneous one.

When heterogeneities are introduced during the miscible displacement, the viscous fingering is exacerbated, and depending on the degree of heterogeneity, the diffusion may not be fast enough to disperse such fingering. We have learned this to be true from the field implementation of miscible CO_2 flooding that has generally shown mobility control issues. Therefore, the presence of heterogeneities is believed to have a role in the reduction of the gap between the residual oil saturation reached by the polymer aided WAG when compared with the conventional WAG, when we changed from homogeneous to heterogeneous rock in our experiments. Therefore, the introduction of further heterogeneities may inverse the gap and cause incremental recovery as polymer is added because the polymer will be able to sweep regions of the reservoir that will not be reached by the non-thickened water, or by the CO_2. Also, it is possible that the higher viscosity water also improves conformance of CO_2. However, it would be challenging to include such heterogeneities in a core flooding experiment because of obvious scaling issues.

Recent simulation work has suggested that polymer aided WAG can recover additional oil when compared with conventional WAG in the NBU. Li et al. (2014) reported ultimate oil recovery factor of 14.3 % of OOIP over water flooding, 7 % higher than the one obtained for conventional WAG. However, the numerical simulation is not supported by any laboratory measurements, and assumes parameters such as polymer adsorption and residual resistance factor (RRF). Besides, the reservoir model is validated using primary and secondary field development, and there is no validation for the complex dynamics of a WAG process even without the presence of the polymers. If no laboratory experiments are matched, it is difficult to know if the numerical simulation is able to capture all the physical phenomena observed, particularly the water shielding and its relationship to rock wettability and viscosity.

Finally, it is believed that a combined approach of laboratory experiments and numerical simulation is required in order to better understand this process. Different experiments under different conditions need to be matched with numerical simulation to make sure that all physical phenomena is correctly reproduced. Only after that, the process can be evaluated in a larger scale, introducing a degree of heterogeneity that cannot be easily handled in the laboratory.

CHAPTER V

CONCLUSIONS

LONG TERM STABILITY OF ACRYLAMIDE BASED POLYMERS IN THE PRESENCE OF CO_2

Carbon dioxide causes further degradation in both, co-polymers of acrylamide and acrylate, and co-polymers of acrylamide and ATBS when compared with the degradation observed under similar conditions in the presence of nitrogen.

The co-polymer of acrylamide and acrylate was able to retain approximately 54% of its original apparent viscosity when aged in the presence of CO_2 during 215 days at reservoir temperature of 122 °F. This means an additional loss of 28% of its original apparent viscosity against samples aged with nitrogen.

The co-polymer of acrylamide and ATBS increased its viscosity to 104% of its original apparent viscosity when aged in the presence of CO_2 during 328 days at reservoir temperature of 122 °F. This means a reduction of viscosity increment of 20% when compared with samples aged with nitrogen.

Both polymers tested can potentially be used for chemically assisted CO_2 WAG, but proper assessment of degradation at the conditions of the reservoir of interest is required. Special attention should be paid in the co-polymer of acrylamide and acrylate since is more susceptible to CO_2 degradation than the co-polymer of acrylamide and ATBS.

Both polymers show a temporary decrease in viscosity retention below the one observed in the long term during the first 18 days of aging in contact with carbon dioxide. This viscosity loss can be compensated with an increase of the concentration of the polymer.

MINIMUM MISCIBILITY PRESSURE

A minimum miscibility pressure (MMP) of 1563 psia was experimentally determined using the slim tubing technique for the system dead NBU crude oil - CO_2 at reservoir temperature of 122 °F.

The MMP experimentally calculated in this work is slightly below previously reported MMP for live NBU crude oil, which is consistent with the reduction in MMP observed with a decrease in solution gas reported in literature.

The use of a shorter column, of 20 ft of length, during the slim tube experiment reduced considerably the time invested in the MMP determination, but the smaller pore volume of approximately 20 cm^3 caused the errors in the measurement of the oil production and the dead volume of the equipment to have a deeper impact in the recovery factors calculated for each slim tube run. An error of 1 cm^3 in the measurement of oil translates into an error of 5% in the recovery factor.

CORE FLOODING EXPERIMENTS

The core flooding experiments performed did not allow reaching a final conclusion regarding the use of polymers as water thickeners during CO_2 WAG EOR given the difficulty of introducing meaningful heterogeneities in a laboratory scale.

In a homogeneous media, the dispersion of viscous fingering in the CO_2 - oil advance front as a consequence of a diffusive phenomenon caused by CO_2 and crude oil miscibility, and low advance flow rate, leads to high oil recovery, in the order of 90 % of OOIP. Under this condition, the use of WAG and polymer assisted WAG reduces the effectiveness of the process as the presence of mobile water limits the ability of CO_2 to contact and displace some of the oil.

The presence of heterogeneities reduces the ability of the crude oil – CO_2 miscibility to disperse the viscous fingering in the advance front. When a critical degree of heterogeneity is reached, the use of polyacrylamides as water thickeners can contribute to recovery by helping the thickened water to contact oil than would not be contact by CO_2 and non-thickened water due to their lower viscosity.

Under immiscible conditions, the viscous fingering in the CO_2 – oil displacement front reduces the recovery by causing low sweep efficiency and early CO_2 breakthrough. The use of WAG improves mobility and sweep efficiency resulting in an increase in oil recovery. The addition of polymer for water thickening was not observed to provide significant improvement to the process. However, as in the miscible case, the increase in the degree of heterogeneity can offer an opportunity for the thickened water to increase recovery as is able to reach oil that cannot be reached by either CO_2 or regular water, due to their lower viscosity.

REFERENCES

Al-Assi, A. A., G. P. Willhite, D. W. Green et al. 2009. Formation and Propagation of Gel Aggregates Using Partially Hydrolyzed Polyacrylamide and Aluminum Citrate (in English). *SPE Journal* **14** (03): 450-461.

Anderson, W. 1986. Wettability Literature Survey- Part 2: Wettability Measurement (in English). *Journal of Petroleum Technology* **38** (11): 1246 - 1262.

ASTM Standard D1193-06(2011). "Standard Specification for Reagent Water". 2011. West Conshohocken, PA. www.astm.org.

Audibert, A., J. F. Argillier. 1995. Thermal stability of sulfonated polymers. Proc., SPE International Symposium in Oilfield Chemistry San Antonio, TX.

Behzadi, S., B. F. Towler. 2009. A New EOR Method. Proc., SPE Annual Technical Conference and Exhibition, New Orleans, Louisiana.

Boneau, D. F., R. L. Clampitt. 1977. A Surfactant System for the Oil-Wet Sandstone Of the North Burbank Unit (in English). *Journal of Petroleum Technology* **29** (05): 501-506. https://www.onepetro.org/journal-paper/SPE-5820-PA.

Caudle, B. H., A. B. Dyes. 1958. Improving Miscible Displacement by Gas-Water Injection. Proc., 32nd Annual Fall Meeting of Society of Petroleum Engineers Dallas, USA.

Christopher, R. H., S. Middleman. 1965. Power-Law Flow through a Packed Tube (in English). *Industrial & Engineering Chemistry Fundamentals* **4** (4): 422-426. http://dx.doi.org/10.1021/i160016a011.

CoreLab. 2010. Minimum Miscibility Pressure and Solubility Swelling Study for tthe North Burbank Unit Field, PENCOR Advanced Fluid Studies, Houston, Texas (03/02/2010).

Craft, B. C. 1991. *Applied petroleum reservoir engineering*. Englewood Cliffs, N.J., Prentice Hall (Reprint).

Dean, E. W., D. D. Stark. 1920. A Convenient Method for the Determination of Water in Petroleum and Other Organic Emulsions (in English). *Journal of Industrial & Engineering Chemistry* **12** (5): 486-490. http://dx.doi.org/10.1021/ie50125a025.

Donaldson, E., R. Thomas, P. Lorenz. 1969. Wettability Determination and Its Effect on Recovery Efficiency (in English). *SPE Journal* **09** (01): 13-20.

Dong, M., S. Huang, R. Srivastava. 2000. Effect of Solution Gas in Oil on CO_2 Minimum Miscibility Pressure (in English). *Journal of Canadian Petroleum Technology* **39** (11).

Ekundayo, J. M., S. G. Ghedan. 2013. Minimum Miscibility Pressure Measurement with Slim Tube Apparatus - How Unique is the Value? Proc., SPE Reservoir Characterization and Simulation Conference and Exhibition.

Enick, R. M., D. K. Olsen, J. R. Ammer et al. 2012. Mobility and Conformance Control for CO_2 EOR via Thickeners, Foams, and Gels -- A Literature Review of 40 Years of Research and Pilot Tests. Proc., SPE Improved Oil Recovery Symposium, Tulsa, Oklahoma.

Glass, O. 1985. Generalized Minimum Miscibility Pressure Correlation (includes associated papers 15845 and 16287) (in English). *SPE Reservoir Engineering* **25** (06): 927-934.

Green, Don W.Willhite, G. Paul. 1998. *Enhanced oil recovery*, Vol. vol. 6, x, 545 p. Richardson, TX: SPE textbook series ;vol. 6 (Reprint).

Herschel, W., R. Bulkley. 1926. Konsistenzmessungen von Gummi-Benzollösungen (in German). *Kolloid-Zeitschrift* **39** (4): 291-300. http://dx.doi.org/10.1007/BF01432034.

Hinkley, R. E., L. A. Davis. 1986. Capillary Pressure Discontinuities and End Effects in Homogeneous Composite Cores: Effect of Flow Rate and Wettability. Proc., SPE Annual Technical Conference and Exhibition, New Orleans, Louisiana.

Holm, L. W., V. A. Josendal. 1982. Effect of Oil Composition on Miscible-Type Displacement by Carbon Dioxide (in English). (1): 87-98. http://www.onepetro.org/mslib/app/Preview.do?paperNumber=00008814&societyCode=SPE.

Jain, R., C. S. McCool, D. W. Green et al. 2005. Reaction Kinetics of the Uptake of Chromium (III) Acetate by Polyacrylamide (in English). *SPE Journal*.

Jenneman, G. E., P. D. Moffitt, G. R. Young. 1996. Application of a Microbial Selective-Plugging Process at the North Burbank Unit: Prepilot Tests (in English). *SPE Production & Facilities* **11** (01): 11 - 17. https://www.onepetro.org/journal-paper/SPE-27827-PA.

Journal, Oil & Gas. 2012. Survey: Miscible CO_2 now eclipses steam in US EOR production. *Oil & Gas Journal*, 2012 Apr 02, 56-57.

Kheradmand, H., J. Francois, V. Plazanet. 1988. Degradation of acrylamide–sodium acrylate copolymer in aqueous solution (in English). *Journal of Applied Polymer Science* **36** (7): 1583-1600. http://dx.doi.org/10.1002/app.1988.070360706.

Kratky, O., H. Leopold, H. Stabinger. 1974. Devices for Measuring Density. United States Patent No. 3910101

Lake, Larry W. 2010. *Enhanced oil recovery*. Richardson, TX, Society of Petroleum Engineers (Reprint).

Levitt, D., G. A. Pope. 2008. Selection and Screening of Polymers for Enhanced-Oil Recovery. Proc., SPE/DOE Symposium on Improved Oil Recovery, Tulsa, Oklahoma, USA.

Li, W., Z. Dong, J. Sun et al. 2014. Polymer-Alternating-Gas Simulation:A Case Study. Proc., SPE EOR Conference Oiland Gas West Asia, Muscat, Oman.

Littmann, W. 1988. *Polymer flooding*. Amsterdam, The Netherlands Elsevier (Reprint).

Manji, K. H., B. W. Stasiuk. 1988. Design Considerations For Dome's David Alkali/Polymer Flood (in English). *Journal of Canadian Petroleum Technology* **27** (03).

Moffitt, P. D., D. R. Zornes, A. Moradi-Araghi et al. 1993. Application of Freshwater and Brine Polymer Flooding in the North Burbank Unit, Osage County, Oklahoma (in English). *SPE Reservoir Engineering* **8** (02): 128 - 134. https://www.onepetro.org/journal-paper/SPE-20466-PA.

Muller, G. 1981a. Thermal stability of high-molecular-weight polyacrylamide aqueous solutions (in English). *Polymer Bulletin* **5** (1): 31-37. http://dx.doi.org/10.1007/BF00255084.

Muller, G. 1981b. Thermal stability of polyacrylamide solutions: effect of residual impurities in the molecular-weight-degradation process upon heating (in English). *Polymer Bulletin* **5** (1): 39-45. http://dx.doi.org/10.1007/BF00255085.

Mungan, N. 1969. Rheology and Adsorption of Aqueous Polymer Solutions (in English). *Journal of Canadian Petroleum Technology* **08** (02): 45-50. https://www.onepetro.org/journal-paper/PETSOC-69-02-01.

Nadeson, G., Z. Md. Zain, S. G. Sayegh et al. 2001. Assessment of Dulang Field Immiscible Water-Alternating-Gas (WAG) Injection Through Composite Core Displacement Studies. Proc., SPE Asia Pacific Improved Oil Recovery Conference, Kuala Lumpur, Malaysia.

Pandey, A., D. A. Beliveau, D. W. Corbishley et al. 2008. Design of an ASP Pilot for the Mangala Field: Laboratory Evaluations and Simulation Studies. Proc., SPE Indian Oil and Gas Technical Conference and Exhibition, Mumbai, India.

Pang, H. W., P. D. Fleming, D. F. Boneau. 1981. Design Of Preflush For Commercial Scale Polymerflood In The North Burbank Unit. Proc., SPE/DOE Enhanced Oil Recovery Symposium, Tulsa, Oklahoma.

Ramsden, D. K., K. McKay. 1986. The degradation of polyacrylamide in aqueous solution induced by chemically generated hydroxyl radicals: Part II—Autoxidation of Fe2+ (in English). *Polymer Degradation and Stability* **15** (1): 15-31. http://www.sciencedirect.com/science/article/pii/0141391086900030.

Ryles, R. G. 1987. Chemical Stability Limits of Water-Soluble Polymers Used in Oil Recovery Processes.

Seright, R.S., A. Campbell, P. Mozley et al. 2010. Stability of Partially Hydrolyzed Polyacrylamides at Elevated Temperatures in the Absence of Divalent Cations (in English). *SPE Journal* (2): pp. 341-348. http://www.onepetro.org/mslib/app/Preview.do?paperNumber=SPE-121460-PA&societyCode=SPE.

Sheng, J. 2011. *Modern chemical enhanced oil recovery theory and practice*, Gulf Professional Pub (Elsevier) (Reprint).

Sorbie, K. S. 1991. *Polymer-improved oil recovery*. Boca Raton, Florida, CRC Press (Reprint).

Stalkup, F. I. 1970. Displacement of oil by Solvent at High Water Saturation (in English). *SPE Journal* **10** (04): 337-348. https://www.onepetro.org/journal-paper/SPE-2419-PA.

Steffe, J. 1996. *Rheological Methods in Food Process Engineering*, 2nd Edition edition. East Lansing, MI, Freeman Press (Reprint).

Trantham, J. C., P. D. Moffitt. 1982. North Burbank Unit 1,440-Acre Polymer Flood Project Design. Proc., SPE Enhanced Oil Recovery Symposium, Tulsa, Oklahoma.

Valbuena, E., M. A. Barrufet. 2013. A generalized partial molar volume algorithm provides fast estimates of CO_2 storage capacity in depleted oil and gas reservoirs (in English). *Fluid Phase Equilibria* **359** (0): 45-53. http://www.sciencedirect.com/science/article/pii/S037838121300424X.

Yang, S. H., L. E. Treiber. 1985. Chemical Stability of Polyacrylamide Under Simulated Field Conditions. Proc., SPE Annual Technical Conference and Exhibition, Las Vegas, NV.

Yuan, H., R. T. Johns, A. M. Egwuenu et al. 2005. Improved MMP Correlations for CO_2 Floods Using Analytical Gasflooding Theory (in English). *SPE Reservoir Evaluation & Engineering* (5): pp. 418-425. http://www.onepetro.org/mslib/app/Preview.do?paperNumber=SPE-89359-PA&societyCode=SPE.

Zhang, Y., S. S. Huang, P. Luo. 2010. Coupling Immiscible CO_2 Technology and Polymer Injection to Maximize EOR Performance for Heavy Oils (in English). *Journal of Canadian Petroleum Technology* **49** (5): pp. 25-33. http://www.onepetro.org/mslib/app/Preview.do?paperNumber=SPE-137048-PA&societyCode=SPE.

Zhang, Y., P. Luo, S. S. Huang. 2010. Improved Heavy Oil Recovery by CO_2 Injection Augmented with Chemicals. Proc., International Oil and Gas Conference and Exhibition in China, Beijing, China.

Zornes, D. R., A. J. Cornelius, H. Q. Long. 1986. An Overview and Evaluation of the North Burbank Unit Block A Polymer Flood Project, Osage County, Oklahoma. Proc., International Meeting on Petroleum Engineering, Beijing, China.